The Pennsylvania State University

The Graduate School

College of Engineering

# VERIFICATION OF LAMINAR AND TRANSITIONAL FLOW SIMULATIONS IN POROUS MEDIA WITH NEK5000

A Thesis in

Nuclear Engineering

by

David M. Holler



Submitted in Partial Fulfillment

of the Requirements

for the Degree of

Master of Science

May 2016

The thesis of David M. Holler was reviewed and approved* by the following:

Kostadin N. Ivanov

Special Signatory

Professor and Chair of Nuclear Engineering

North Carolina State University

Thesis Co-Advisor

Maria N. Avramova

Special Signatory

Associate Professor of Nuclear Engineering

North Carolina State University

Thesis Co-Advisor

Arthur T. Motta

Professor and Chair of Nuclear Engineering

Pennsylvania State University

Justin Thomas

Special Signatory

Manager, Engineering Simulations

Argonne National Laboratory

Aleksandr Obabko

Special Signatory

Principal Computational Engineer

Argonne National Laboratory

* Signatures are on file in the Graduate School.

# ABSTRACT

This thesis is a numerical study of laminar flow through a microscopic section of porous media using simulations performed by the computational fluid dynamics solver Nek5000. The theoretical origins of Nek5000 are discussed, as well as the methods utilized to compute solutions. Motivations for this research, including porous media model implementation and selected reactor core design, are discussed. A literature review was conducted in order to determine the current level of work being done in this field. Most of the current efforts are aimed towards understanding turbulence, since the laminar regime is much more understood. Laminar and transitional relations for porous media parameters are presented and evaluated for a unit cell created with Nek5000 using the already included meshing utility. The mesh contained 2,304 spectral elements, with a polynomial order of 7 and an integration order of 11 for the convective terms. All results show strong correlation to the applied Reynolds number, none of which are linear. The reduced pressure drop, permeability, and form coefficient were found to have strong correlations in the laminar region ($Re < 0.1$). All three parameters had weaker correlations in the regions of transition ($Re > 0.1$). The transition from viscous to form drag dominated flow is predicted to occur at a Reynolds number of 8, which is within an order of magnitude of the prediction of the onset of transition by the other three parameters. The results of this thesis are then compared with the solutions to potential flow, and show little departure from the expected velocity profiles. Conclusions and recommendations follow, where it is suggested that this study be redone with more geometry refining and also evaluated with a turbulence model.

# TABLE OF CONTENTS

# LIST OF FIGURES

# LIST OF TABLES

# NOMENCLATURE

Symbols

$\nabla$ = del operator

$\boldsymbol{u}$ = velocity

$\rho$ = density

$p$ = pressure

$\mu$ = kinematic viscosity

$q'''$ = volumetric heat flux

$T$ = temperature

$k$ = thermal conductivity

$C_p$ = specific heat

$D$ = drag

$\eta$ = similarity variable

$\nu$ = dynamic viscosity

$c$ = local speed of sound

$\phi$ = porosity

$K$ = permeability

$C$ = form coefficient

$D_h$ = hydraulic diameter

$\tau_w$ = wall shear stress

$L$ = characteristic length

$U$ = free-stream velocity

$\delta$ = boundary layer thickness

Dimensionless Quantities

$Re$ = Reynolds number

$M$ = Mach number

$Po$ = Poiseuille number

Subscripts

$p$ = pore

$D$ = diameter based

$e$ = effective

$st$ = steady

$0$ = based on reference temperature

# ACKNOWLEDGEMENTS

This work would not have been possible without my dedicated teachers and advisers, and the faculty at the Argonne National Laboratory. I also thank the user community of Nek5000 for their input, and I sincerely hope to continue to be a part of the Nek5000 project. Finally, I thank my family who has provided unbounded support for me throughout my academic career.

# Chapter 1: Introduction

Nek5000 is an experimental computational fluid dynamics (CFD) research code developed at Argonne National Laboratory. It simulates unsteady incompressible flow with spectral elements, and is written in the Fortran 77 (F77) and C languages. Steady flow, which will be approximated later in this thesis, can be simulated by using constant values for all input parameters and allowing the calculation to run long enough for the velocity and pressure solutions to converge. The entire Nek5000 project is based on Nekton 2.0, the first three-dimensional (3-D) spectral element solver [1], developed by Paul Fischer et al. Unlike finite elements, spectral elements use high-order polynomials within the elements themselves to calculate a solution. It is this polynomial approach that allows Nek5000 to find multiple solutions within one element, and sets its spectral element method apart from the more common counterpart, the finite element method. Finding multiple solutions within one element can lead to a higher accuracy solution, but the real attraction of Nek5000 is its scalability. Nek5000 is easily converted from serial use (one processor) to parallel use (more than one processor) with the editing of a few lines of code. So far, Nek5000 has been shown to work on just over 1 million cores (processors), and will certainly continue being tested as parallel computing capabilities are extended even further.

Nek5000 is, at its most basic level, a laminar flow solver. While a few turbulent cases have been developed and released with the repository, they are difficult to implement because of the complexity of turbulence itself. Fortunately, this study will consider laminar and transition flow, the latter of which will simply be a test of the limits in Nek5000.

Nek5000 was built for scalability and efficiency. The efficiency of calculation time in Nek5000 can be determined by examining the end of one of the log file created during each calculation performed. Normally, two log files are created. One is simply called *logfile*, and it contains the log of every calculation performed in the current working directory (provided the user has not wiped the directory).

The second file, which is named with numerical extensions that depend on the number of CPUs and iterations, will contain only the most recent calculation. The built-in calculation of the central processing unit (CPU) time per step per grid point at the end of the file provides the user with a convenient method of approximating how efficient the calculation was. Examining this parameter is a simple method of benchmarking with the Nek5000 solver, which is explained in the next paragraph.

Nek5000 can also be used for benchmarking purposes. The foremost reason it is capable of benchmarking is the information at the end of the log file mentioned in the previous paragraph. More important is the CPU time per step per grid point parameter. If the user correctly identifies the proper number CPUs, polynomial order, and integration order, then this parameter can be held relatively constant. Once this parameter is held constant across several calculations and CPUs, then the units can be properly compared.

The entire Nek5000 repository is open-source, which means that any user can download and implement it. This not only helps build a community of skilled users, but allows any user with sufficient interest to learn about Nek5000 and its overall process. Other software packages such as OpenFOAM are also open-source, but have been built for different uses. For example, OpenFOAM was built to execute smaller-scale problems with relative ease. This does not mean OpenFOAM is not capable of large scale calculations, but it is not parallelized as easily as Nek5000 is.

Nek5000 can be coupled with third-party meshing utilities such as ICEM and Cubit. Coupling to MATLAB is also available. However, a mesh used for a Nek5000 calculation must be composed entirely of hexahedrons, or elements with six sides. Mesh generators such as Cubit and ICEM are more powerful and can provide acceptable meshes, but the coupling procedure can prove to be difficult. OpenFOAM and the ANSYS suite do not have the hexahedral mesh requirement, which gives them more flexibility. As one can imagine, a complex geometry may be hard to replicate with hexahedrons. OpenFOAM and

ANSYS both support tetrahedral (elements with four sides) meshes, which can prove to be easier to generate. The convergence of the subsequent calculation may be more difficult with tetrahedral meshes, but the solvers that use them are normally used for steady-state calculations. The steady-state assumption is an efficient way to converge a solution with a lower quality mesh.

## 1.1 Motivation for Research

The primary motivation for this research is for the application to thermal-hydraulic analysis of nuclear reactor core designs. One core design to which Nek5000 could be used to evaluate is the 350-megawatt Modular High-Temperature Gas Reactor (MHTGR-350), which has already been documented and benchmarked [2].

Prismatic HTGRs such as this work by forcing inert, high-temperature gas through numerous coolant channels in graphite fuel elements. The use of graphite is appropriate, because the inert gas does not react directly with carbon and it is much more temperature resistant than the light water reactor (LWR) material of choice, zirconium alloy. Also, the graphite acts as a neutron moderator, similar to the water in LWR cores. Radiation effects and steam ingress are problems known to occur in HTGR designs, but there are drawbacks to any design.

A standard fuel element of the MHTGR-350 core has 318 channels, which are occupied by fuel, burnable poison, control rods, or coolant. Figure 1 shows the design of a standard fuel element in the MHTGR-350 design, where the units are in inches. More information about the design of this specific fuel element can be found in Appendix A.

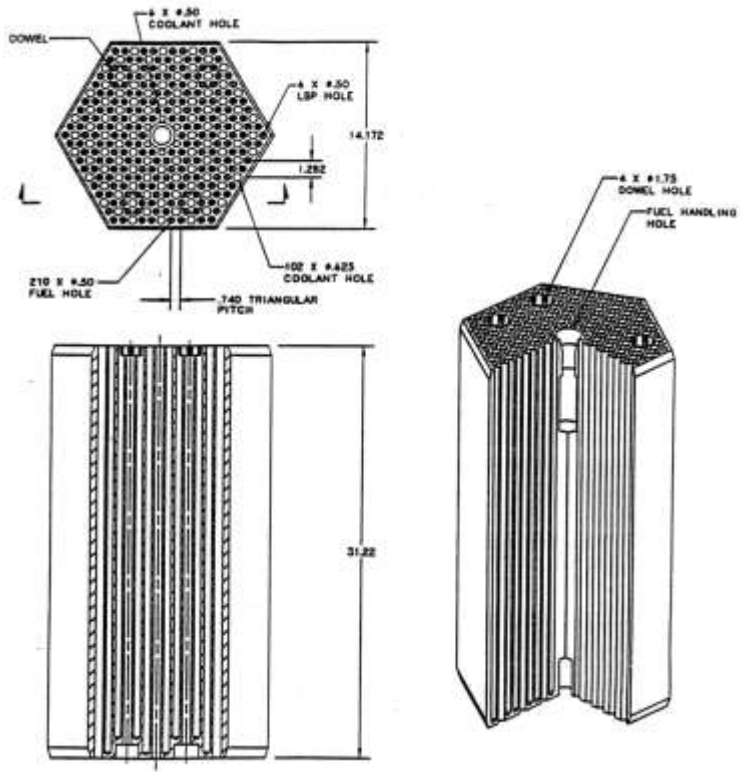


Figure 1. Standard fuel element design of the MHTGR-350 reactor core.

In some designs, specifically the high-temperature gas reactor (HTGR) designs, it is appropriate to approximate the coolant flow in the core region with a porous medium. The validity of this approximation arises from the relatively simplistic fluid flow geometry through the core, and its computational cost reduction. Since 3-D CFD codes employ full velocity and pressure solutions in a given field, an application to the aforementioned prismatic core would yield 108 coolant channel solutions. Much of these solutions would be incredibly similar, which creates somewhat of a redundancy that could possibly be avoided with a porous medium approximation.

The design process of anything requires a certain level of safety analysis, and nuclear reactors are certainly not exempt from this stipulation. Past accidents and phenomena have taught the industry that safety is indeed of paramount importance. For this reason, accident tolerance and scenarios are simulated before full reactor designs ever see production.

One of the scenarios that is unique to HTGR designs is the flow reversal during a loss of flow (LOF) accident. In the HTGR core, coolant is normally routed through the core from top to bottom. Figure 2 shows how this cooling normally takes place. The yellow arrows indicate the intended coolant flow path.

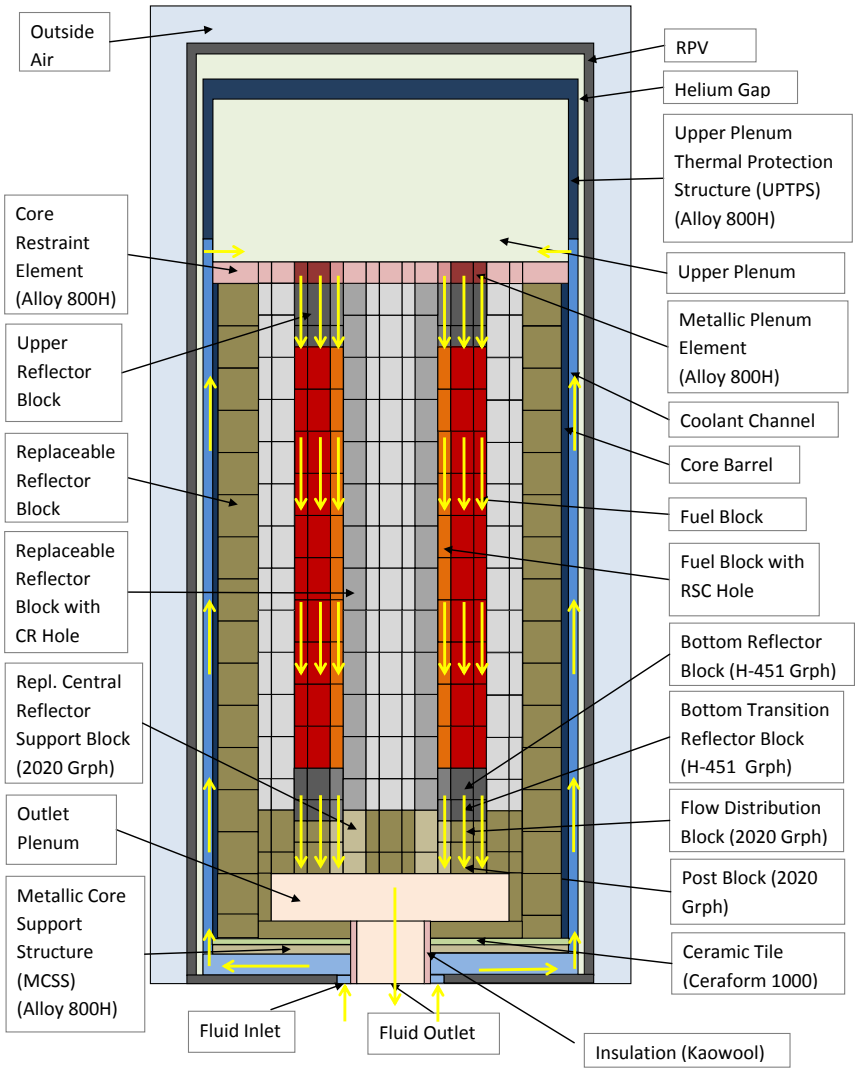


Figure 2. Design of MHTGR-350 core with normal coolant flow pattern.

In the LOF situation, something has caused the normal flow pattern to stop, and eventually it reverses in the HTGR core due to the buoyancy instabilities of natural convection. In order to simulate this accident scenario, a solver would need a conjugate heat transfer infrastructure in place to accurately solve the

continuity, momentum, and energy equations of fluid flow. Conjugate heat transfer is needed because of the interface between solid and fluid found in this core (and all other fluid-cooled cores). Nek5000 has a conjugate heat transfer example in its repository, which could be used to simulate this LOF accident scenario. Modification would be necessary, no doubt, but the benefit of using Nek5000 for a calculation such as this accident scenario is its accuracy and efficiency.

Aside from accident scenario testing, reactor cores also need to be evaluated for efficiency before and during operation. In HTGR core designs, one type of inefficiency that can become a problem is coolant flow outside its own channels. Also known as core bypass flow, this phenomenon can lead to overall inefficiency of the core system and possibly an unwanted rise in temperature. If too large of a fraction of coolant is traveling between fuel elements and not in the channels it was designed to use and extract heat from, then this unwanted temperature rise can lead to an accident. If Nek5000 was used to simulate core bypass flow, then a porous media model would not be appropriate. An approximation method like that used in porous media models is would simply not allow any investigations into core bypass flow.

The other source of motivation for porous media modeling in relatively simple flow geometry is the possibility of decreasing computational cost. Since the onset of the recent surge in simulation development, every project is scrutinized for efficiency. Full-model CFD evaluation for a design such as the HTGR would lead to a high computational cost, but it may be possible to decrease that cost by a significant margin. By using a porous media approximation for flow through the coolant channels, the local solution is homogenized and approximated with one model. This model is not being developed in this thesis; it is merely a test of Nek5000. The current laminar and turbulent models need testing to determine if they are capable of representing a porous model.

Another reactor core design that Nek5000 could eventually be applied to is the light water reactor (LWR) core. While this reactor design has been around for over 40 years and is well observed and tested, there is always room for improvement. Currently, one of the most accessible codes is a one-dimensional solver known as TRACE. This code comes in different versions and forms, including the Symbolic Nuclear Analysis Package (SNAP), but the methods of solving for the desired variables are all in one dimension. In many cases, one dimension provides enough insight and is also very efficient. However, if more detail is desired, then one-dimension is not enough.

One of the main problems with simulating LWR designs with computer code is their two-phase behavior. Even the pressurized water reactor (PWR), a type of LWR, the primary system of which is kept at a high pressure (around 2250 psi) to maintain liquid-phase water, includes a few components (pressurizer, secondary loop) that contain both liquid and vapor phases of water. A considerable amount of research has been conducted so far into this matter, and it is of no doubt that this issue will continue to be explored. One possible way to simulate a core design such as that found in the PWR is with Nek5000. Nek5000 is currently a one-phase solver, but a two-phase model is being developed. Turbulence is almost always assumed to exist when dealing with complex systems such as reactor cores, so a suitable turbulence model would also need to be included.

This section would not be complete if the current applications of Nek5000 to reactor systems were not discussed. One of the current areas of research is the sodium fast reactor (SFR), which employs fast (high-energy) neutrons, as opposed to thermal neutrons, to react with fuel that is cooled with liquid sodium. This reactor design has been shown to work, but as one can imagine, liquid sodium would be difficult to use as a coolant. Sodium was chosen for its heat transfer characteristics, which are inherently better for this application than gas or water.

## 1.2 Outline of Thesis

Chapter 2 reviews literature related to the current study of incompressible turbulent flow in porous media. Current work for practical use in reactor designs is presented, along with arguments concerning its use for this thesis. Publications in the areas of CFD, porous media, and turbulence in porous media are evaluated for their use, along with usable information from each work.

Chapter 3 provides a description of the implications and consequences of the assumption of incompressible flow. The conservation equations of continuity and momentum for a one-phase medium are presented to provide a basis of understanding of the fluid flow present in this study. Other ways of expressing the indications of incompressible flow are also considered.

Chapter 4 contains an overview of porous media, along with details about the porous media parameters to be calculated. A scientific definition of porous media is presented, which is more useful than the basic definition that precedes it. Perhaps the most important part of Chapter 4, however, is where the relations for permeability and form coefficients are discussed which will both be evaluated in this study.

Chapter 5 describes the experimental approach of this thesis, which is comparable to most CFD problem solving methods. The geometry and mesh are presented, along with the steps used in the terminal to compile, solve, and process the study. The *Lineout* measurement mode of VisIt is also described in this chapter.

Chapter 6 discusses the results found by applying Reynolds numbers ranging from 0.01 to 25 to the test section. The results were found to be separable, and the reason and process of doing so are discussed. The overall results are plotted first, and then each group of results is presented and evaluated separately. Boundary layer theory is also included as a comparison to the early methods of solving laminar velocity profiles.

Chapter 7 is the final chapter of this thesis, and it contains the conclusions and recommendations drawn from the process and results of this experiment. Suggestions for future studies with Nek5000 are included, along with possible improvements of this study.

# Chapter 2: Literature Review

There are a number of models for flow in porous media available, depending on the application. The most relevant to nuclear reactor core flow is the model proposed by Chandesris et al [3]. The flow was modeled axially in a rod bundle, which is conspicuously similar to the core assembly inside an LWR. Here, they heed the advice of Pedras and de Lemos [4] and apply the time-averaging operator first, then the volume average. Such a process was shown to account for the turbulence inside the pores [3], which the opposite process did not. While the work of Chandesris et al [3] is more applicable to three-dimensional situations, this thesis is limited to only two dimensions for simplicity.

A dissertation by Clifford [5] was by far the most influential work to this thesis. Clifford developed a thermal-hydraulic solution method for the MHTGR-350 design that considered all scales present in the reactor core, including micro-scale heat conduction within the fuel pellets. However, the most pertinent part of this work is section 5.2, where a porous medium test was performed to determine if the porous medium parameters were correlated to the Reynolds number. Multiple macroscopic parameters were found to be correlated to the Reynolds number, including the pressure drop, along with the turbulent kinetic energy and the corresponding dissipation rate. However, one main difference exists between Clifford's work and this thesis. The porous medium models in the former work were developed for compressible flow, which is a required condition in the case of HTGR designs. This thesis will only be concerned with incompressible flow; it is a requirement of using the Nek5000 solver. The result of using the incompressible flow assumption is that the numerical solution will be inherently different than a compressible flow solution.

After review of the dissertation mentioned in the previous paragraph, more complete definitions of the porous medium parameters for incompressible flow were sought out. A publication by Narasimhan [6] provided such definitions. In particular, the permeability and form coefficients are presented from an

experimental perspective, which gives the reader a clear understanding of their origins. The relations for these coefficients will be used to determine the aforementioned permeability and form coefficients later in this thesis, but not in the same manner as Clifford [5].

The consultation of a publication of de Lemos [7] reveals the complexity of applying turbulence models to porous media. Upon further reading, however, the inspiration for the study by Clifford [5] became apparent. In the fourth chapter of de Lemos, a similar porous media study was performed to determine the coefficient $c_k$ , which is essential for a closed equation model in turbulent problems. Overall, this study was a continuation of work by Pedras and de Lemos [8], which was repeated by Clifford and now the current thesis.

# Chapter 3: Incompressible Flow

Incompressible flow is a condition that occurs when the local density of a substance does not depend on pressure. The density can then be thought of as a function of other system variables, such as temperature. If the system is isothermal, however, then density can be approximated as a constant value. Even if small fluctuations in temperature exist, the density of a substance is usually approximated to be constant for the sake of simplicity. Since Nek5000 is an incompressible solver, it is helpful to simplify the problem and use isothermal conditions.

One of the most common indications of incompressible flow is when the divergence (dilatation) of the velocity is equal to zero, which is also known as the continuity equation. This is represented by Equation (3.1), which is in vector notation. The divergence represents the sum of the changes of each velocity component in their respective directions. This equation does not change when applied to turbulent flows.

$$\boldsymbol{\nabla} \cdot \boldsymbol{u} = 0 \tag{3.1}$$

A better explanation of Eq. 3.1 can be made when one considers the mathematical implications of vector divergence. When fluid velocity is the vector quantity in question, then one may say that the volumetric strain rate is zero. This is a much more concrete statement about the physical consequences of Eq. (3.1).

Equations (3.2) and (3.3) are the equations for momentum and energy balance for incompressible flow, taken directly from the Nek5000 equation manual [9]. Neither of these equations are averaged or decomposed yet; their purpose is to show the consequences of incompressibility (the density term is now present outside all derivatives).

$$\rho\left(\frac{\partial \boldsymbol{u}}{\partial t} + \boldsymbol{u} \cdot \nabla \boldsymbol{u}\right) = -\nabla p + \nabla \cdot \mu(\nabla \boldsymbol{u} + (\nabla \boldsymbol{u})^T) + \boldsymbol{f} \tag{3.2}$$

$$\rho C_p \left( \frac{\partial T}{\partial t} + \boldsymbol{u} \cdot \nabla T \right) = \nabla \cdot k \nabla T + q''' \tag{3.3}$$

The letter ***f*** represents a user-specified forcing function, which will be zero throughout this study. External (body) forces are assumed negligible (except any user-defined function).

All three equations can also be non-dimensionalized, which makes the overall computation process simpler. For example, the momentum equation can be multiplied by $\frac{L}{U^2}$ to obtain a dimensionless form.

$$\left\{ \frac{L}{U^2} \right\} \left\{ \rho \left( \frac{\partial \boldsymbol{u}}{\partial t} + \boldsymbol{u} \cdot \nabla \boldsymbol{u} \right) \right\} = \left\{ \frac{L}{U^2} \right\} \{ -\nabla p + \nabla \cdot \mu (\nabla \boldsymbol{u} + (\nabla \boldsymbol{u})^T) + \boldsymbol{f} \} \tag{3.2.1}$$

$$\frac{\partial \boldsymbol{u}}{\partial t} + \boldsymbol{u} \cdot \nabla \boldsymbol{u} = -\frac{1}{\rho} \nabla p + \frac{1}{Re} \nabla^2 \boldsymbol{u} + \boldsymbol{f} \tag{3.3.1}$$

The pressure and forcing function have now been scaled by $\frac{1}{\rho}$, and the viscosity term is replaced by the reciprocal of the Reynolds number.

Incompressibility can also be determined from the availability of a thermodynamic pressure solution. If one does not exist, then only a mechanical (mean) pressure can be calculated, since there is no equation of state to determine a thermodynamic pressure [10].

Another way to approximate incompressibility for a fluid is to use a relation to the respective Mach number. In general, Nek5000 can use only fluids for which Equation (3.4) is valid. This is a much simpler (although inaccurate) approach to incompressibility, especially when only a target or maximum velocity is known.

$$M \equiv \frac{U}{c} < 0.1 \tag{3.4}$$

# Chapter 4: Porous Media

Porous media can be defined as solid structures interconnected voids, but the definition presented by Narasimhan [6] provides a much clearer, scientific insight. According to this text, a porous medium can be defined as "a region in space comprising of at least two homogeneous material constituents, presenting identifiable interfaces between them in a resolution level, with at least one of the constituents remaining fixed or slightly deformable." In this experiment, one substance (solid) will remain fixed while the other will flow around it (gas).

## 4.1 Laminar Flow in Porous Media

In order to find the permeability and form coefficient presented in Chapter 3 of Narasimhan's text [6], the flow must be assumed to be viscous and have constant properties. This is only possible in the laminar flow regime, where the pore Reynolds number must be less than 0.1. Equation (4.1.1) shows how the pore Reynolds number is found. The pore diameter, $D_p$ , is the characteristic length between the fixed constituents. The nominal fluid velocity is given by *U,* and the kinematic fluid viscosity is represented by *v*.

$$Re_D \equiv \frac{UD_p}{\nu} < 0.1 \tag{4.1.1}$$

The Reynolds number is a dimensionless quantity widely used to determine if a certain flow is laminar or turbulent. From a more basic perspective, however, the Reynolds number can be defined as the ratio of inertial to viscous effects. This would lead one to the conclusion that laminar flow is dominated by viscous effects, while turbulence is dominated by inertial effects.

When flow is established in a section of porous medium, the momentum equation for a porous medium is valid (Equation (4.1.2)). Here, the effects of porosity ($\phi$), permeability (*K*), and form (*C*) are apparent. The fluid density, $\rho_f$ , and the effective dynamic viscosity, $\mu_e$ , are also now separated from the nominal

density and viscosity due to effects found only in porous media.

$$\frac{\rho_f}{\varphi}\left[\frac{\partial \boldsymbol{u}}{\partial t} + \boldsymbol{u}\cdot\nabla\mathbf{u}\right] = -\nabla p + \mu_e\nabla^2\boldsymbol{u} - \frac{\mu}{K}\boldsymbol{u} - \rho C|\boldsymbol{u}|\boldsymbol{u} \tag{4.1.2}$$

For laminar flow, Narasimhan [6] presents multiple relations for calculating both the permeability and form coefficient. One method of determining the permeability is Darcy's Law, which is shown as Equation (4.1.3). This is a constitutive relation which actually defines the permeability, *K*.

$$K = \frac{\mu}{\Delta P_v}U \tag{4.1.3}$$

Here, the pressure drop term represents the change in pressure in the length of flow occupied by porous media alone. It may be desirable to have a relationship that is more general and applicable to more situations.

Another method of determining the permeability is shown by Equation (4.1.4). This relationship is derived from Eq. (4.1.2), after assuming steady, fully-developed, and unidirectional flow. The viscous and form terms are also assumed to be negligible.

$$\frac{\Delta P}{L} = \frac{\mu}{K}U \tag{4.1.4}$$

In this expression, *L* is the characteristic length of the porous medium, and *U* is the mean flow speed. Since the viscous and form effects have been accounted for—i.e. neglected—this expression can be deemed to be less restrictive.

Until now, the measured pressure drop would include all effects encountered between the pressure taps on a test channel. If only the secondary (viscous) effects are desired in the determination of the permeability, then Equation (4.1.5) would be appropriate. This expression subtracts the wall friction

contribution of pressure change from the total pressure change (across the porous medium), with the use of the Poiseuille number (Equation (4.1.6)).

$$K = \left[\frac{\Delta P_{cv}}{L\mu U} - \frac{2Po}{\varphi D_h^2}\right] \tag{4.1.5}$$

$$Po = \frac{2\tau_w D_h}{\mu \boldsymbol{u}} \tag{4.1.6}$$

In these expressions, $D_h$ is the hydraulic diameter, and $\tau_w$ is the shear stress at the wall. Upon inspection, one can see that the function of the Poiseuille number is to compare the friction diffusion with the viscous diffusion effects near the wall surface. While Eq. (4.1.5) would suit a real system better, this experiment will use Eq. (4.1.4) because of its looser confines.

Now that an acceptable expression for the permeability has been found, it is necessary to present an expression for the form coefficient. Both parameters are necessary for the analysis of the laminar capabilities of Nek5000.

If a similar procedure to that of Eq. (4.4) is followed to find a form coefficient, then Equation (4.1.7) would be the result. The left-hand side of the momentum equation has again been ignored, along with viscous and permeability effects. In actuality, this would require a measured or calculated pressure drop due to form drag alone, which is denoted as $\Delta P_f$.

$$C = \frac{\Delta P_f}{\rho U^2 L} \tag{4.1.7}$$

However, it would be more practical to use an expression that includes the total pressure drop across a test channel, which is what is measured. This approach is similar to that of Eq. (4.1.5), due to the fact that secondary effects have been accounted for. Equation (4.1.8) shows how a corrected form

coefficient is found. The total measured pressure drop is denoted as $\Delta P_m$.

$$C = \frac{1}{\rho U^2}\left[\frac{\Delta P_m}{L} - \frac{\Delta P_{cv}}{L}\right] = \frac{1}{\rho U^2}\left[\frac{\Delta P_m}{L} - \frac{\mu U}{K}\right] \tag{4.1.8}$$

Narasimhan makes it a point to the reader that in a study by Lage et al [11], the permeability and form coefficient should be calculated together using Eqs. (4.1.5) and (4.1.8). This point follows instinct and logic, because it accounts for the porous medium and non-porous sections alone, as opposed to the combination of all effects present. Unfortunately, this study does not include sections of both free flow and porous media, so Eq. (4.1.7) will be used to find the form coefficient.

## 4.2 Flow Transition in Porous Media

In porous media, it is difficult to develop and maintain fully developed turbulent flow. Evaluating turbulent behavior in porous media is also difficult, and both concepts are beyond the experimentation of this thesis. Instead, the transition away from Darcy flow will be predicted with information from Narasimhan [6].

There are several ways to express flow transition, and this study will only be concerned with the transition from a regime dominated by viscous drag to a regime dominated by form drag. The Hazen-Dupuit-Darcy model can be interpreted to express transition, which is the basis of Equation (4.2.1). This equation is also restricted to isothermal flows (hence the "0" subscript), which is exactly the application of this experiment.

$$\left.\frac{\Delta P}{L}\right|_0 = \frac{\mu_0}{K_0} U + \rho_0 C_0 U^2 = D_{\mu_0} + D_{C_0} \tag{4.2.1}$$

Fortunately, a simpler expression is available thanks to scaling analysis by Lage [11]. Here, in Equation (4.2.2), the ratio of the form drag to the viscous drag is found that can ultimately predict the onset of

transition, which is expected to occur when λ is equal to 1. However, this expression is meant for uniform cross-section porous media, which the current microscopic study cannot represent.

$$\lambda = \frac{D_{C_0}}{D_{\mu_0}} = \left(\frac{\rho C_0 K_0}{\mu_0}\right) U \tag{4.2.2}$$

Equation (4.2.2) will be used with the results to predict the onset of transition, but speculation will be necessary because the aforementioned restriction of this prediction.

# Chapter 5: Experimental Methods

The goal of this numerical experiment is to conduct a study similar to that of Pedras and de Lemos [7] [8] and Clifford [5], which should be indicative of future trends in porous media modeling with Nek5000. The trends that are of concern are the successes and problems that will arise after calculation with Nek5000.

This numerical experiment is similar to the standard CFD approach, with a few different steps that are needed to run a Nek5000 simulation. The steps are detailed in the following sub-sections.

## 5.1 Geometry

The geometry for this numerical study was replicated from earlier works by Clifford [5] and Pedras and de Lemos [7] [8]. It is a unit cell in a structure of periodic cylinder arrays, which can be found in structures that use cylindrical columns for support. Figure 3 shows the geometry of this unit cell, where *H* has been set equal to 4 units. The shaded areas represent solid cylindrical structures, while the blank space is fluid.

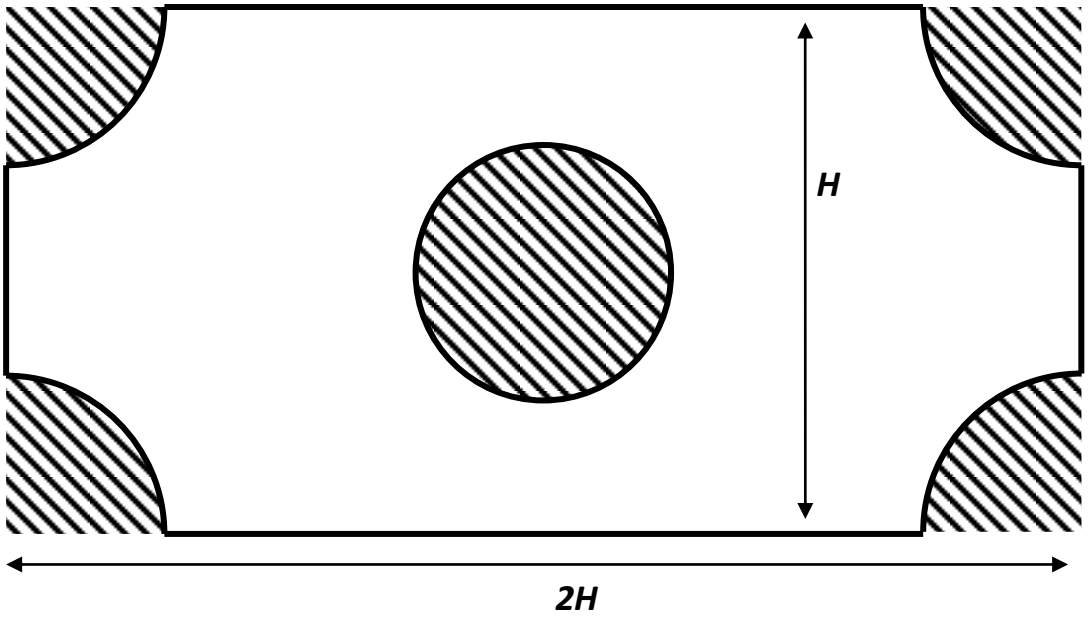


Figure 3. Geometry of test section.

This geometry differs slightly from that of actual periodic arrays, because it does not have a true triangular pitch. The reason for neglecting a true pitch was to simplify the meshing process, which was done manually in Prenek.

## 5.2 Mesh

Meshes are the visual representation of the locations of solutions within a test section. In this experiment, the mesh was constructed manually in the Prenek Graphical User Interface (GUI). Similar to other CFD meshes, the elements of this mesh were purposefully made smaller where more resolution was needed. Figure 4 shows the completed mesh. The element size specifications are necessary, yet somewhat misleading because Nek5000 is a spectral solver.

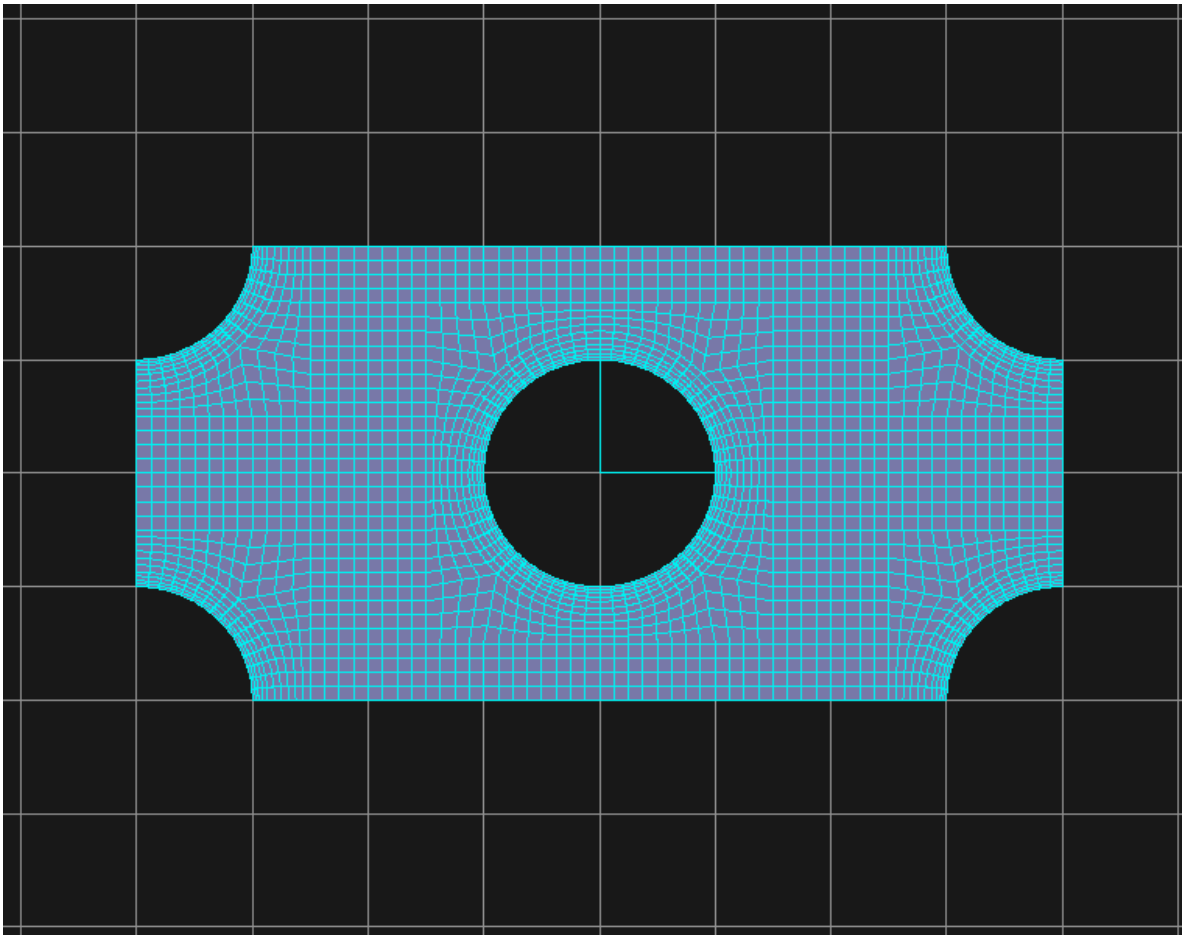

Figure 4. Mesh of test section for simulation.

## 5.3 Boundary Conditions

The boundary conditions in Nek5000 are similar to that of any CFD solver, except special care must be taken when dealing with small elements manually. The top and bottom boundaries were set to a symmetry condition, which is acceptable for this laminar experiment. Errors were present when periodic boundary conditions were used, which is an issue for other CFD solvers as well.

The left and right boundaries of the mesh were set to inlet and outlet, respectively. Nek5000 allows the user to specify a function of velocity at the inlet, but this experiment is only concerned with constant velocities. A constant velocity of 1.0 correlates with the non-dimensional flow equations outlined in an earlier section.

The boundaries of the cylinders have been made walls, where the no-slip condition is enforced. No-slip simply means that all fluid velocities are zero along the wall, and this B.C. is handled well by Nek5000 and other CFD solvers.

## 5.4 Compilation

Nek5000 requires the user to change certain values within its scripts before compilation. First, several parameters within the *.rea* file must be changed to meet the specifications of the experiment. The parameters of concern here are viscosity, number of time steps (NSTEPS), and time step size (DT). The viscosity term is equivalent to the reciprocal of the Reynolds number, which was mentioned in Chapter 3. The number of time steps ranged from 50,000 to 1,125,000 and the time step was held at $10 \times 10^{-6}$ seconds. Appendix B contains this and all other pertinent data from all calculations.

The second file that requires modification is the *SIZE* file. The *SIZE* file contains information about the number of dimensions, solver method, mesh size, and number of processors needed, among other parameters. Since this experiment is two-dimensional, the number of elements in the third dimension

(parameter *lz1*) is set to 1. Also, the global element parameter *lelg* must be equivalent to the number of elements in the mesh (2,304), and the maximum number of processors (parameter *lp*) was 4.

The last file that needs modification is the *.usr* file, which contains the functions and variables solved during execution. The user can set boundary conditions here as well, which is useful if a third-party meshing utility is used. However, the only modifications necessary for this experiment are to ensure that the inlet velocity B.C. of 1.0 is present, and that all initial conditions (I.C.s) are zero. A brief investigation into different I.C.s was performed, and it was determined that zero I.C.s provided the most stable solution.

Unlike some codes, Nek5000 requires extra compilation before execution to build the necessary structures for a solution. This is first done by executing the *genmap* command, which maps the mesh for parallel computation. Then, the *makenek* script, which automatically builds the execution library for a specific calculation, is executed in the working directory. No modifications of the *makenek* script were necessary for this experiment.

## 5.5 Solver Execution

This step uses one of several available scripts within the Nek5000 repository to solve a problem. This numerical simulation employed the most common script, *nekbmpi*. Essentially, the *nekbmpi* script runs a parallel Nek5000 calculation in the background. Initially, however, the foreground version *nekmpi* was used to ensure a stable calculation. After the errors became smaller than the set tolerances, stability was determined to exist and all calculations were put into the background.

## 5.6 Post-Processing

After the calculation is finished, it still needs graphical representation. When using Nek5000, this step is accomplished with VisIt, a visualization tool developed at the Lawrence Liverpool National Laboratory.

Since the only variables calculated for this experiment were pressure and velocity, the analysis in VisIt proved to be relatively simple.

First, while still in the working directory of the Nek5000 calculation, the *visnek* script is run. This script creates a *.nek5000* database file from the *.f00* field files that were created during solver execution. Then, VisIt is opened from the command line and the user can open the database file to view contours and other plots of the pressure and velocity. While viewing the converged contour of pressure, the *LineOut* mode can be activated, creating a one-dimensional line of measurement across the centerline of the test section. This data is automatically plotted, and can then be modified and exported as a data file. In the exported database, it is important to remember that the distance along the line drawn is non-dimensional.

# Chapter 6: Results and Discussion

The first result of concern is the reduced pressure drop found throughout the calculations. Nearly every equation in Chapter 4 contains some relation to the pressure drop across the test section, so it is the first result discussed. Figure 5 shows the correlation of the reduced pressure drop to the applied Reynolds number.

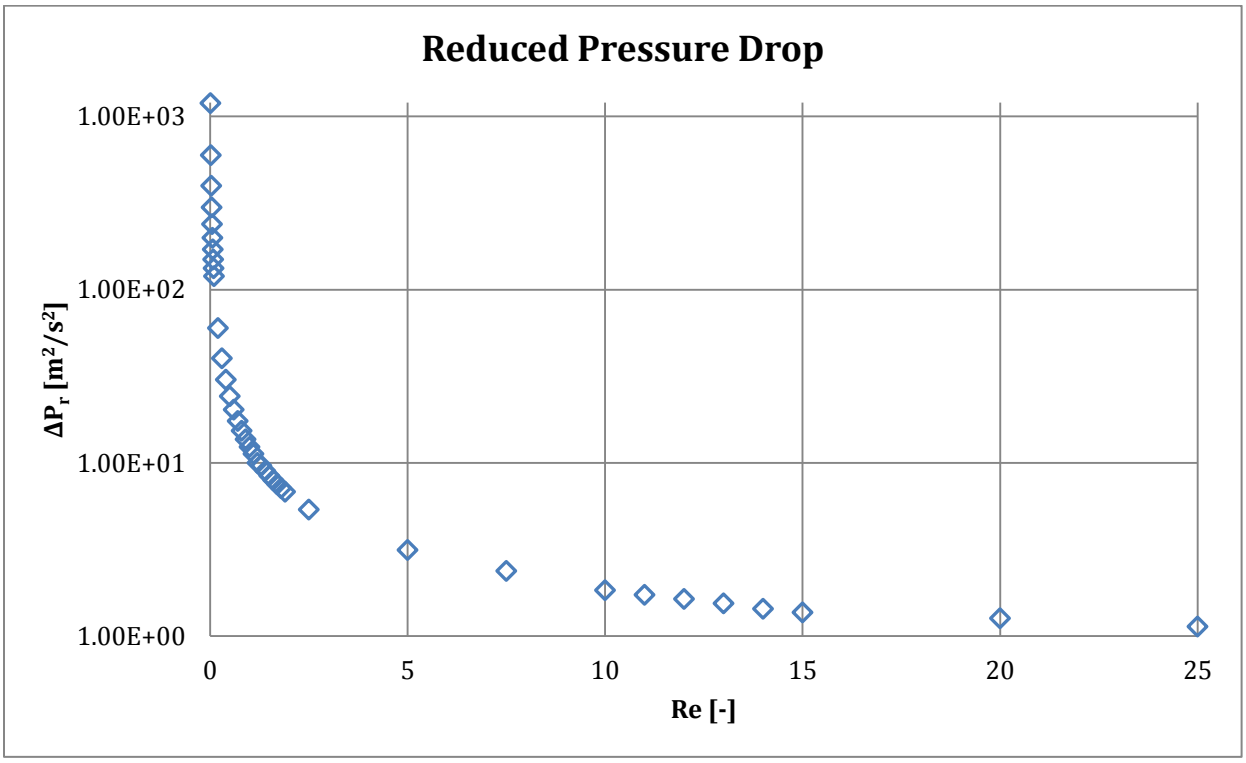


Figure 5. Reduced pressure drop as a function of the applied Reynolds number.

The regions of viscous (*Re < 0.1*) and inertial (*Re > 0.1*) dominated flow are apparent, with notable differences of slope between the regions. The entire data set (presented in Appendix B) can be approximated with a power law function, but the correlation coefficient was found to be 0.9944. Since this correlation coefficient is much smaller than 1 (as far as correlation coefficients go), the viscous and transition regions were examined separately, and verification of the requirement that *Re < 0.1* was performed.

The deviation from viscous flow in the transitional region was expected, because it includes inertial effects, and the transition away from laminar flow exhibited a strong presence. Figure 6 shows the converged results of the magnitude of velocity at a Reynolds number of 25, which shows separation behind the center cylinder and a dramatic decrease in boundary layer thickness on the leading edges. The highest velocity (red) is 1.316, while the lowest (blue) is zero.

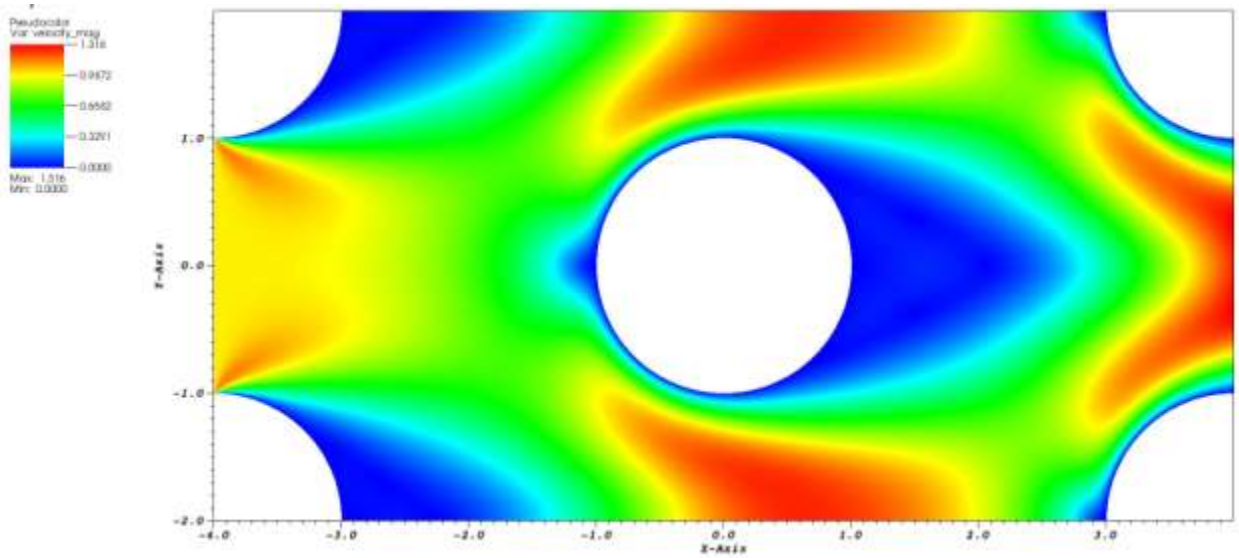


Figure 6. Filled contour (pseudocolor) plot of velocity magnitude at *Re = 25*.

Permeability was the next result under investigation. As predicted, Nek5000 showed a correlation, albeit weaker than the reduced pressure drop, between permeability and the Reynolds number. Figure 7 shows the calculated permeability for the range of input Reynolds numbers.

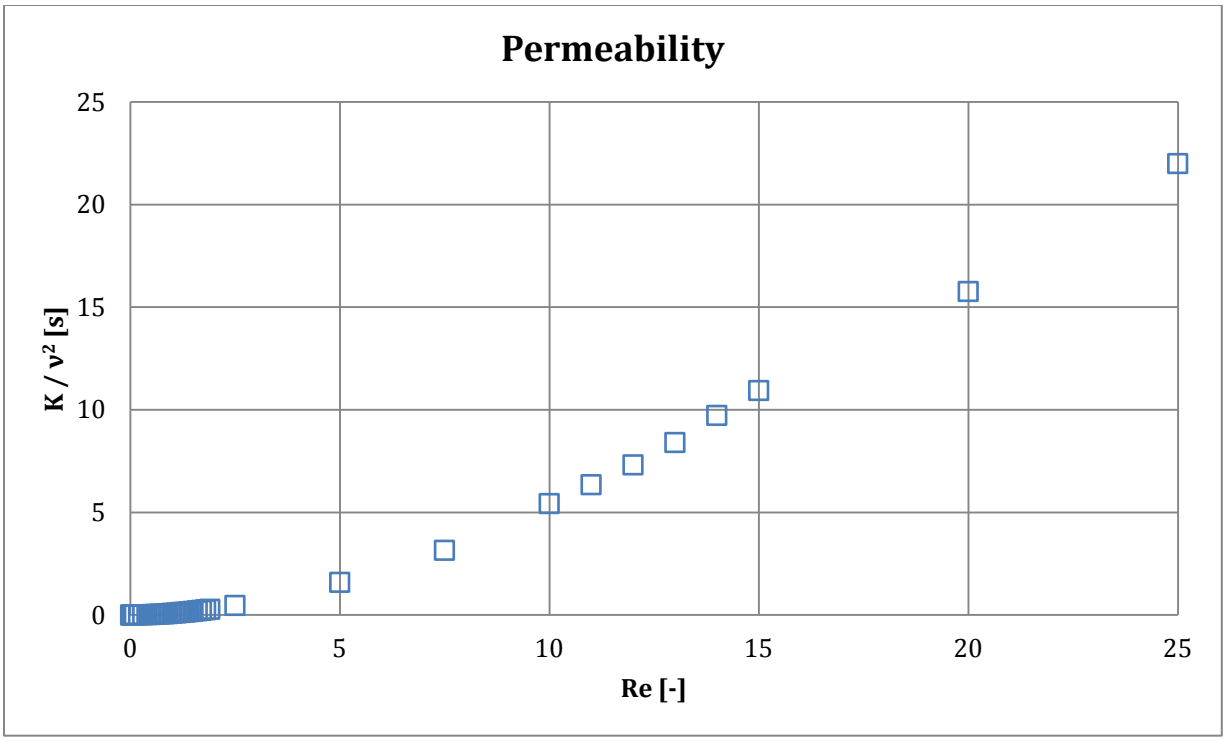


Figure 7. Permeability as a function of applied Reynolds number.

The best correlation that could be found was a high-order polynomial but a polynomial correlation is not desirable for this application because the parameters being calculated are valid for the laminar region only. If a polynomial approximation was used, then the trend line equation would eventually approach an asymptote, which is detrimental to the future of this study. To accommodate the absence of an acceptable correlation for all permeability values, each flow regime will be examined in the same manner as that of the reduced pressure drop.

The next parameter to be calculated is the form coefficient, with the use of Eq. (4.1.7). Figure 8 shows the results, with the dependent variable actually being the product of the form coefficient, kinematic viscosity, and mean flow speed. This product was formed because of its direct dependence on the Reynolds number, and because this experiment was non-dimensionalized for simpler computation. A physical experiment would include a real value for all parameters, including viscosity and flow speed.

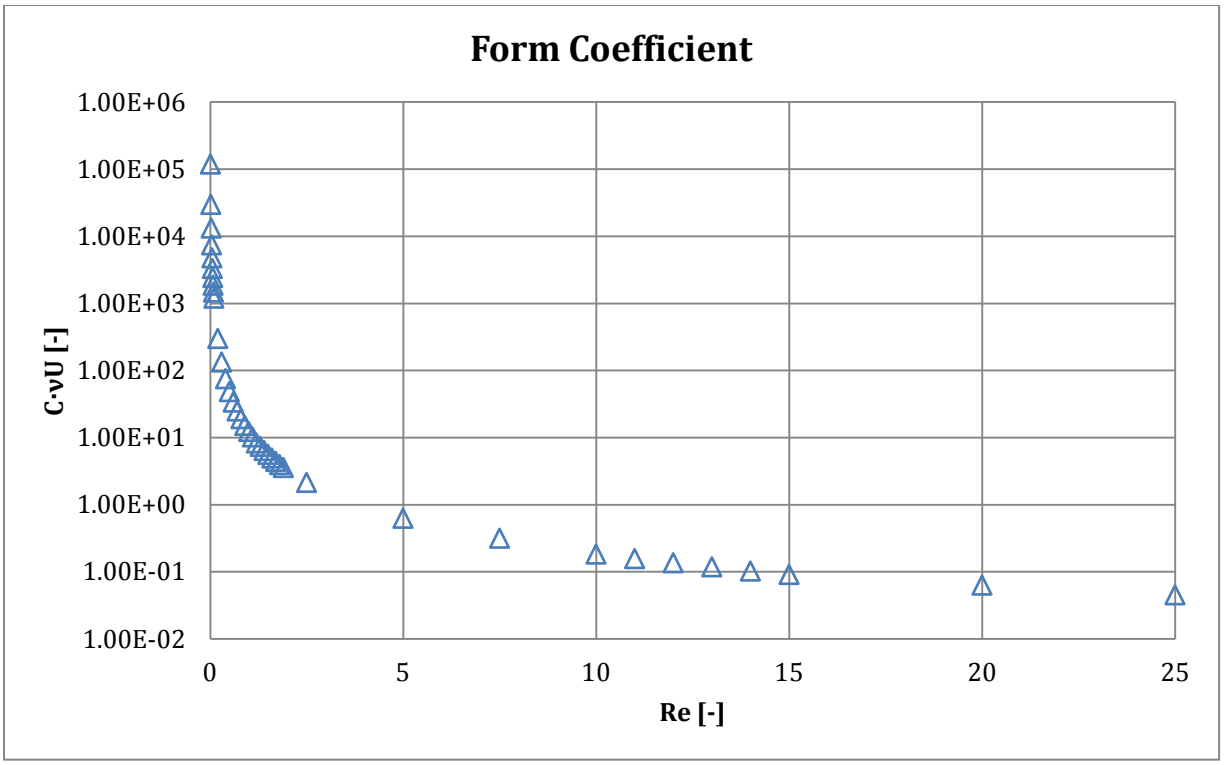


Figure 8. Form coefficient as a function of applied Reynolds number.

Figure 8 also shows that the form coefficient is not a realistic parameter at low Reynolds number values. Even when multiplied by the kinematic viscosity and flow speed, the form coefficient will still be quite large. For example, the working fluid can be air at room temperature, which has an approximate kinematic viscosity of $10^{-5}$. The characteristic length is the diameter of the pore, which is equal to the diameter of the cylindrical structures in this case ($D_p$ = 2.0). At a Reynolds number of 0.01, the mean flow speed is equal to 5.0E-7. According to these results, the corresponding form coefficient would then be over 2E16. Therefore, the form coefficient in this range is not realistic but will still be plotted to reinforce this conclusion.

The last parameter to investigate with the overall results is the ratio of viscous and form drag effects, denoted by λ in Eq. (4.2.2). The length of the test section was set at 8 units, which have remained dimensionless throughout this experiment for the sake of computation time and breadth of application. Figure 9 is a plot of the drag ratio, which is conspicuously linear. The correlating linear equation is

shown in the upper right corner of the figure. The transition from viscous to form-dominated drag is approximated at a Reynolds number of 8.

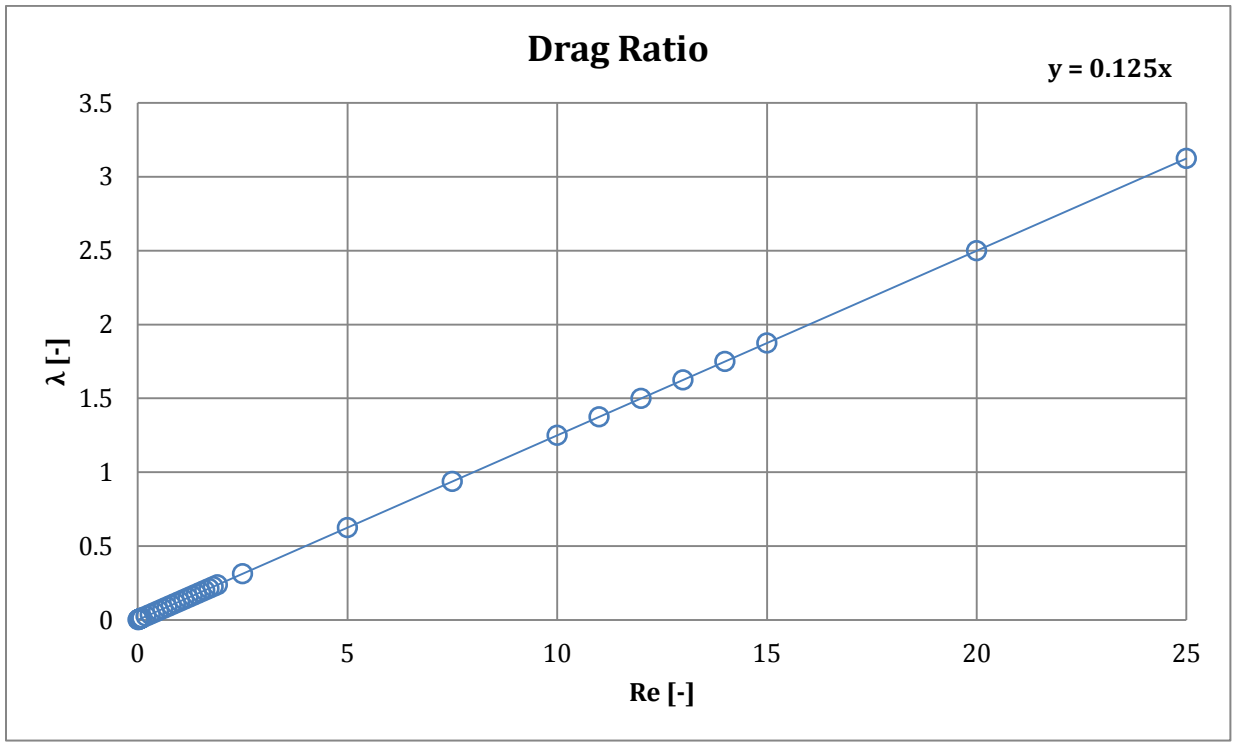


Figure 9. Viscous-to-form drag ratio as a function of Reynolds number.

The reason for the absolute linearity found in Fig. 9 is the calculation method of the permeability and the form coefficient. Non-dimensional components were used in the absence of actual fluids and their corresponding properties. However, the results plotted in Fig. 9 are not completely inconsistent with the other figures. Fig. 9 may predict the transition at *Re* = 8.0, which appears to be an overshoot, but is within an order of magnitude of the inflection points found in Figs. 5 and 8. Overall, the drag ratio does not work in non-dimensional form.

After examination of the overall results, it was deemed necessary to investigate the effects simulated by Nek5000 in separate flow regions. Table 1 shows how the overall results were classified into different regions of flow.

Table 1. Classifications of simulated flow regions.

| Region | Lowest *Re* | Highest *Re* |
|---|---|---|
| Laminar | 0.01 | 0.09 |
| Transition I | 0.2 | 0.9 |
| Transition II | 1.0 | 2.5 |
| Transition III | 5.0 | 25.0 |

This classification was performed based on the behavior found in Figs. 5, 6, and 7. There are clear differences found throughout the data, and the boundaries of each region could still be debatable. However, they will suffice for this experiment.

## 6.1 Laminar Region (*Re < 0.1*)

In tradition of the previous paragraphs, the reduced pressure drop in the laminar region of flow will be examined first. Figure 10 shows a closer look at the laminar region. Here, another power law was used to correlate the data, which is now in the lower right hand corner. A near-perfect fit was found, meaning that Nek5000 shows the expected result of a strong correlation between pressure drop and Reynolds number, especially where the Reynolds number is less than 0.1.

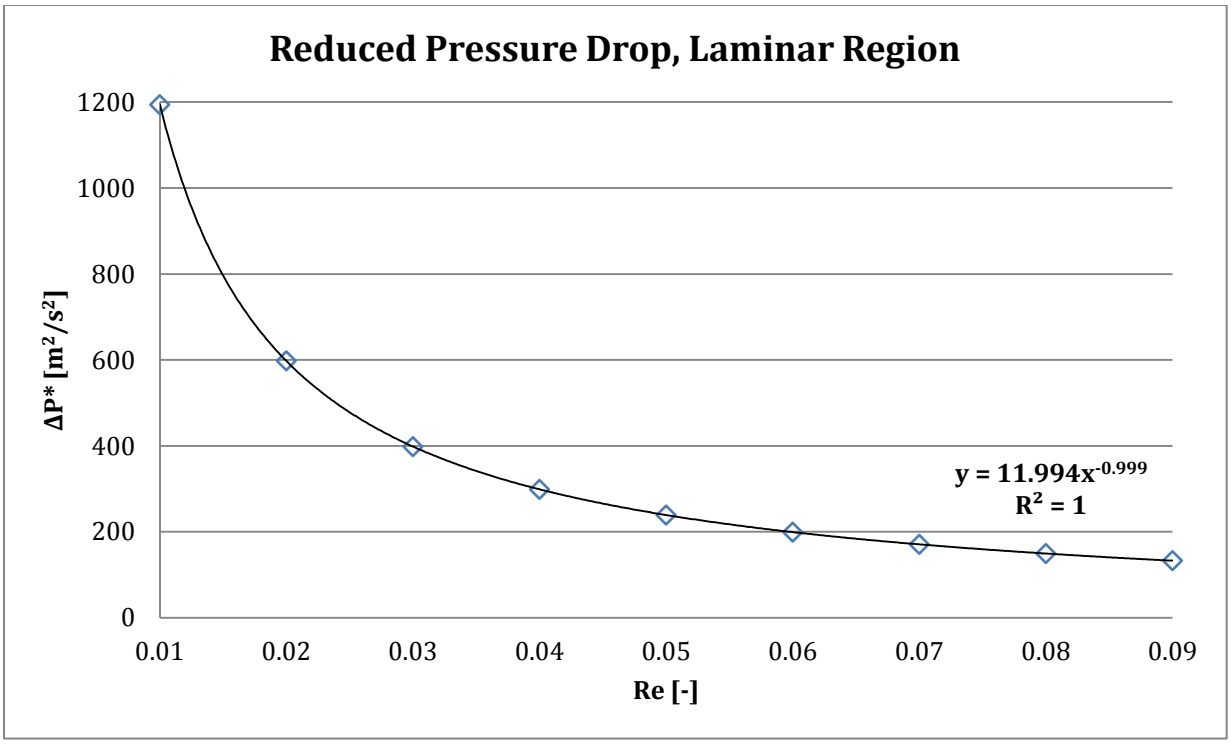


Figure 10. Reduced pressure drop of laminar region.

The reason for this strong correlation found in Fig. 10 is that the laminar region of fluid flow is where exact flow solutions exist. These exact solutions (to continuity and the Navier-Stokes equations in this case) are much easier for Nek5000 to find. The equations are nearly 100% valid, especially with the present assumption of constant properties.

In a similar fashion to Fig. 5, the permeability was closely investigated in the viscous region. Figure 11 shows a near-perfect match of a power law to the permeability. Again, this was expected because of the laminar Nek5000 solver employed and the restrictions on the parameters calculated.

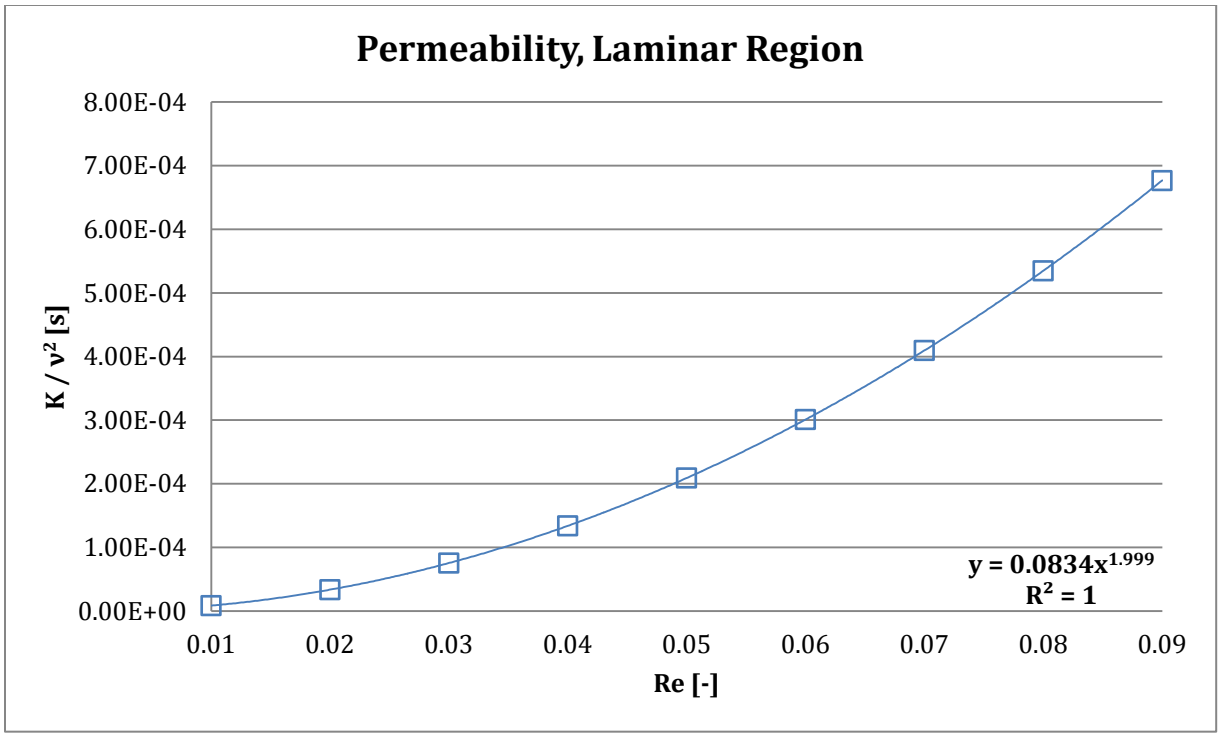


Figure 11. Permeability calculated in the viscous region.

The validity of these permeability values could also be disputed, as was done with the form coefficient values. The microscopic-scale test performed in this study is not something that is ordinarily done with porous media, but is necessary for the future implementation of an accurate porous media model. Further testing and future developments will be reserved for a later section.

The form coefficient in the laminar region has already been deemed unrealistic, but is plotted in Figure 12 for the sake of completeness. Nek5000 seems to be showing that the effects of both the permeability and form coefficient are more applicable to higher Reynolds numbers.

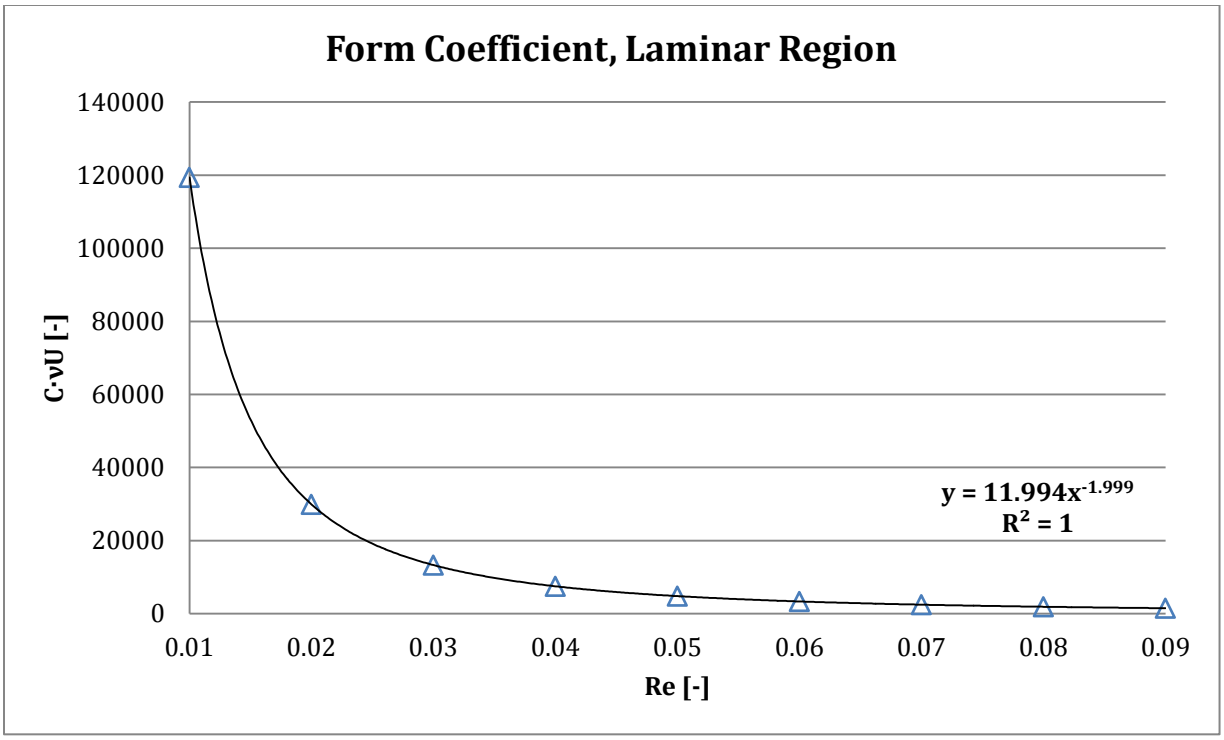


Figure 12. Form coefficient in the viscous region.

Along with completeness, the Fig. 12 was generated to find a correlation between its data points. The correlation, found near the lower right corner, is of an expected value because the data points generated are essentially the reciprocal of the permeability. This only further proves that this study is only preliminary, but essential for full porous media model development.

The viscous region has now been fully evaluated, based on the objectives set forth by this study. Nek5000 shows that it is fully capable of producing strong correlations in this regime, which is important because many applications of a porous media model have characteristic Reynolds numbers of less than 0.1. One such application could be oil extraction from shale formations, where the viscosity can have quite a wide range. However, if the Reynolds number in the reservoir was measured far away from the extraction point, it would be low because of the vast reservoir size. A similar situation can be found in large tanks of water that have small flow exits. The liquid is approximated to be stagnant away from the exit.

## 6.2 Transition Region I (*0.1 < Re < 1.0*)

The next region under consideration is deemed the first region of transition, found between Reynolds numbers of 0.1 and 1.0. The behavior that determined the boundaries was that found at *Re* = 0.1 and *Re* = 2.5. The reduced pressure drop and other parameters evaluated at these values were not consistent with and of a different magnitude than those between 0.1 and 1.0.

The reduced pressure drop was found to have a good correlation with the applied Reynolds number, but not as strong as that found in the viscous region. Figure 13 shows this correlation, along with the approximated equation and its correlation coefficient.

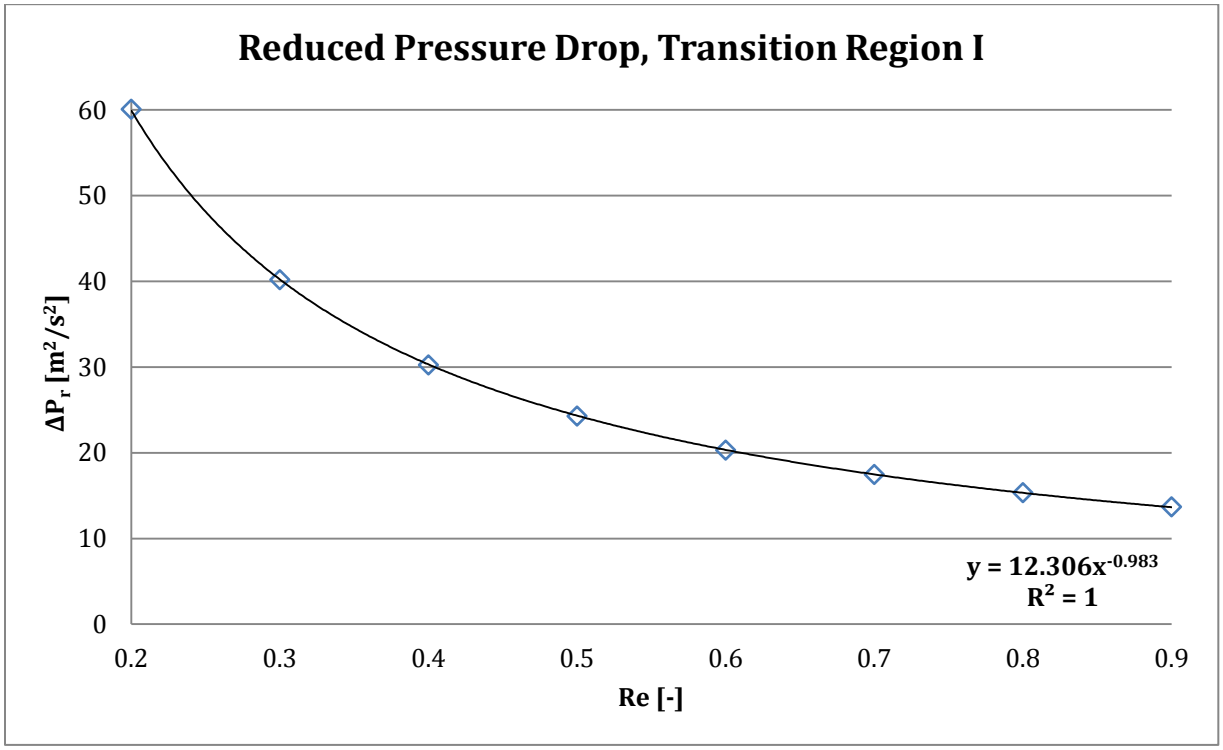


Figure 13. Reduced pressure drop in the first region of transition.

The correlation equation found in the lower right corner of Fig. 13 is different than that found in the viscous region, which was $y = 11.994x^{-.999}$. The difference is small, yet large enough to warrant separate investigations for each region of flow. Also, the correlation coefficient is high enough to prove

that this region contains a strong relationship between the Reynolds number and reduced pressure drop.

The permeability values calculated for Transition Region I also has a strong correlation to its applied Reynolds numbers. Figure 14 shows this correlation, along with the approximated equation and correlation coefficient of the data set.

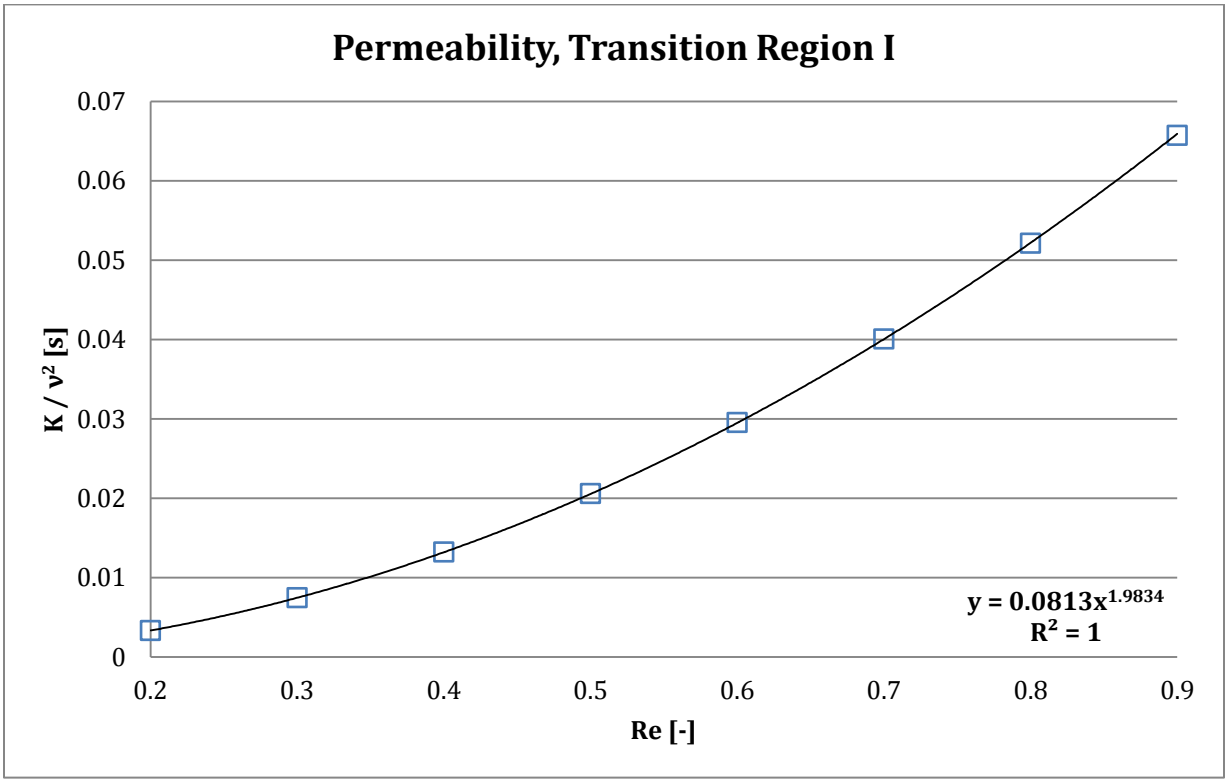


Figure 14. Permeability for first region of transition.

The coefficients in the approximation equation have both decreased since moving away from the laminar region of flow. These smaller numbers correlate to a larger overall increase of permeability throughout this flow region, which is about 0.06. This trend is expected to continue, but only evaluation will provide confirmation of this expectation. Finally, since the simulations have now left the laminar region, the permeability values are beginning to reach realistic values for applications of Nek5000.

The form coefficient of the first transition region is plotted next, in Figure 15. The approximated power law and correlation coefficient are in their usual place, the lower right corner.

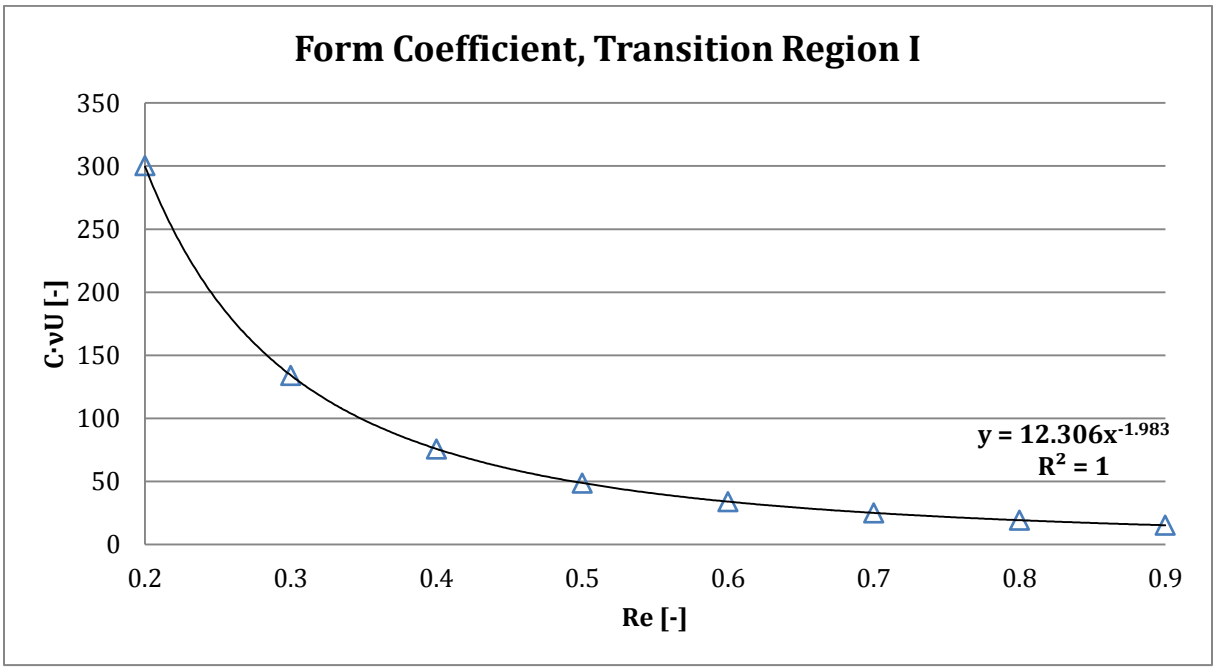


Figure 15. Form coefficient of the first transition region.

In contrast to the results of permeability, the coefficients in the approximation equation in Fig. 15 have increased after moving out of the viscous region. This effect was expected, since the overall experimental results have already shown an inverse relationship between the Reynolds number and form coefficient. Regardless, it is pertinent that each region is examined for its behavior before an approximation of the entire experimental data set is formed.

## 6.3 Transition Region II ($1.0 < Re < 2.5$)

The second region of transition, classified as the flow regime between Reynolds numbers of 1.0 and 2.5, will now be evaluated.

The first parameter, as usual, is the reduced pressure drop. Figure 16 shows how it relates to the applied Reynolds number in this region. While it may not seem significant at the moment, the changes in the approximated equations between regions are important.

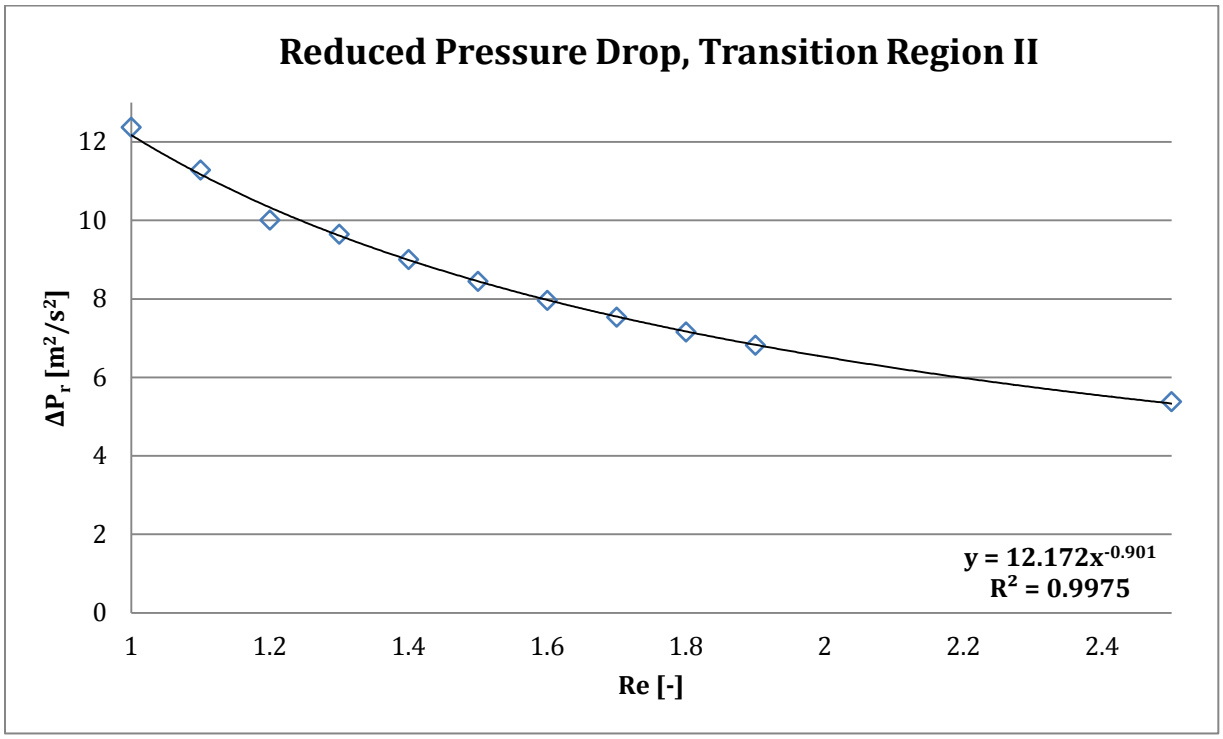


Figure 16. Reduced pressure drop in the second region of transition.

One may notice that a few of the data points in Fig. 16 do not appear to have been completely converged. Error in these calculations is attributed to discrepancies in VisIt, which was used to determine the onset of convergence. Every calculation in this region was simulated with 50,000 time steps, and for the most part, the data points correlate well. Another possibility could be inconsistencies in Nek5000, especially with the onset of transitional flow.

Next, the permeability of the second region of transition is plotted with its correlation equation and coefficient in Figure 17. The direct relationship between applied Reynolds number and permeability is still apparent, but at a different level than that of the previous sections.

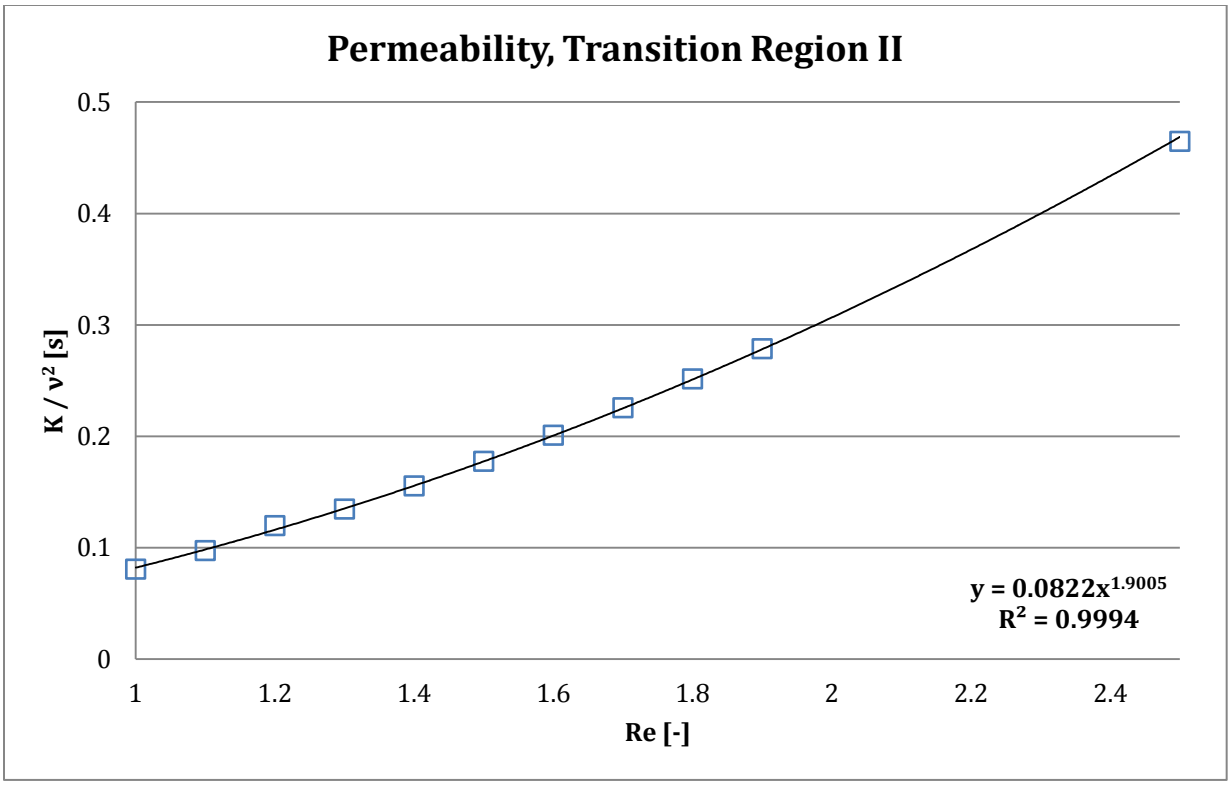


Figure 17. Permeability of second transition region.

A few data points in this set also appear to not be fully converged. However, their correlation is not as greatly affected due to the method of their calculation. In other words, performing multiplication caused the inconsistencies to smooth out, resulting in a higher correlation coefficient.

The form coefficient for the second transition region is now evaluated. Figure 18 shows the resultant plot of the form coefficient versus the applied Reynolds number. This graph also shows some discrepancies, but the correlation coefficient is still sufficiently high to draw conclusions about the data set.

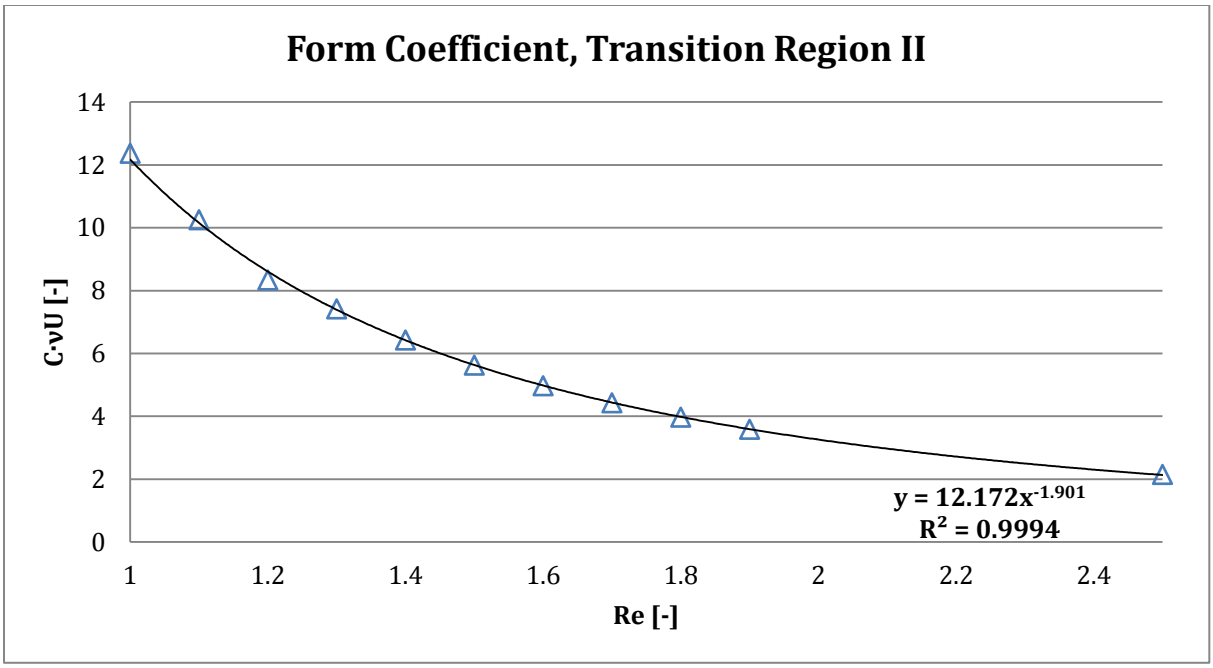


Figure 18. Form coefficient evaluated for the second region of transition.

As previously mentioned, the multiplication (and division) by the applied Reynolds number seems to have provided a smoothing effect on the inconsistent values near the beginning of this data set. Also, all three parameters continued their expected behavior, even through a few questionable results.

The trend of a decreasing form coefficient implies that something else is taking over its effects, which could be the inconsistency of transitional flow itself. It is well known that CFD codes have trouble providing accurate calculations of transitional flow. One possibility is that the form drag is starting to be influenced by inertial effects, and the increasing Reynolds number is certainly a factor. The final region of transition will be evaluated next, which will hopefully provide more insight into this phenomenon.

## 6.4 Transition Region III ($5.0 < Re < 25$)

The third and final region of interest is now under consideration. Before any of the following plots are presented, the prediction of looser correlations within the data is now in effect. After the evaluation of the second region of transition in the previous section, it was shown that inconsistencies are beginning

to appear. These inconsistencies are expected to grow as Nek5000 moves out of the regime that it was designed to solve for.

First, the reduced pressure drop is evaluated. Figure 19 shows how the reduced pressure drop relates to the applied Reynolds number in this region. As predicted, the correlation coefficient has decreased, possibly due to an inaccurate assignment of boundaries to this region.

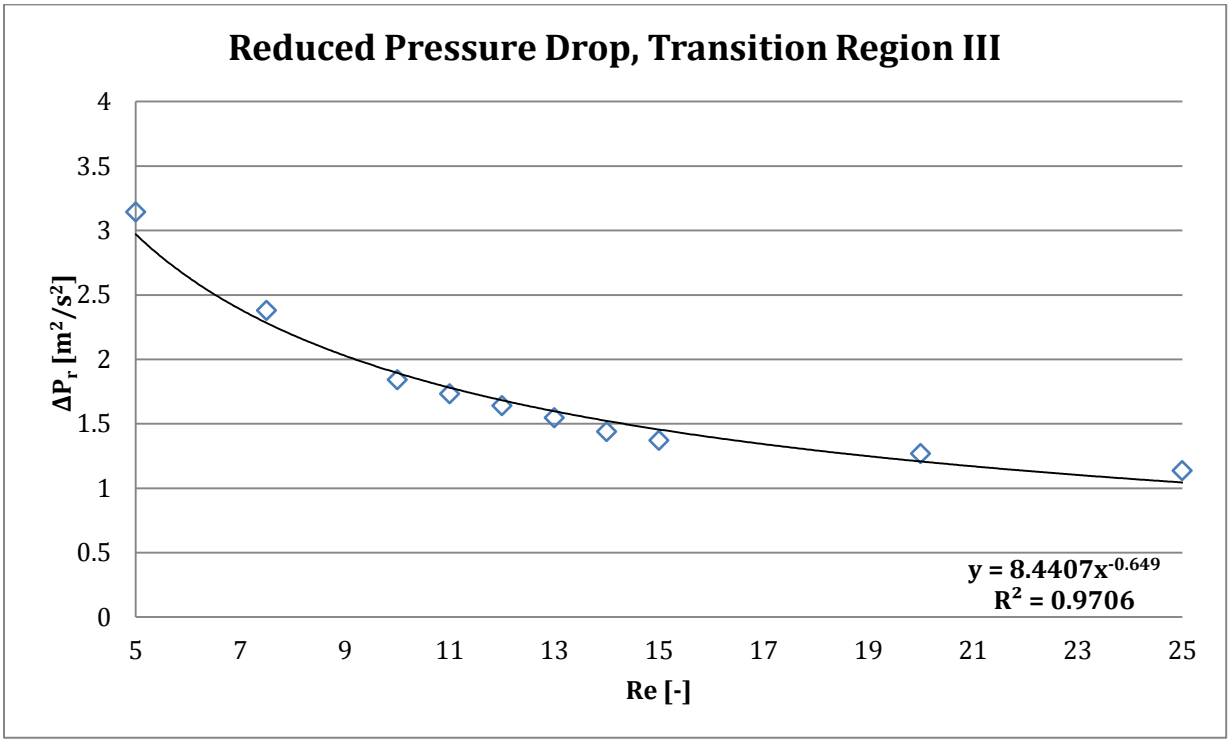


Figure 19. Reduced pressure drop in third region of transition.

Since the convergence of this data set was confirmed, the reason for its relatively low correlation coefficient must be related to transitional flow itself. Absolute correlation past the laminar region was not expected, but it was nearly obtained in the first region. Also, the coefficients in the trend line equation are now substantially lower than in the laminar region. There is now no question that the Reynolds number has now left the laminar region.

The permeability also now shows the effects of transitional flow, which can be seen in Figure 20. Even though the correlation coefficient is above 0.99, the data are conspicuously outside the trend line.

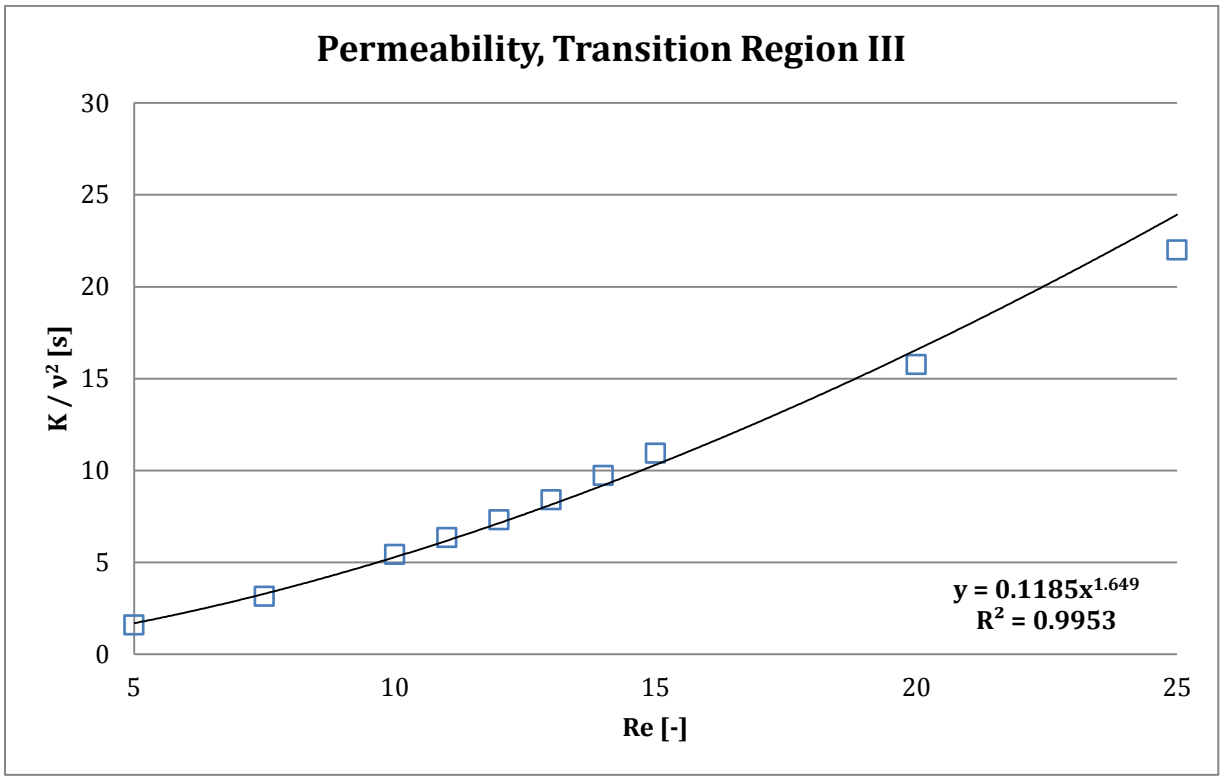


Figure 20. Permeability in the third region of transition.

Another probable reason for the lower correlation may lie in the calculation method of the permeability. It was noted in Chapter 4 that the better relations for permeability and other parameters could not be used because of the nature of this experiment. Compromises such as this are always present in relatively simple studies such as this thesis.

Finally, the last plot under consideration is the form coefficient of the third region of transition. Figure 21 shows this plot, along with its trend line equation and correlation coefficient. The effects of transition flow are apparent here as well.

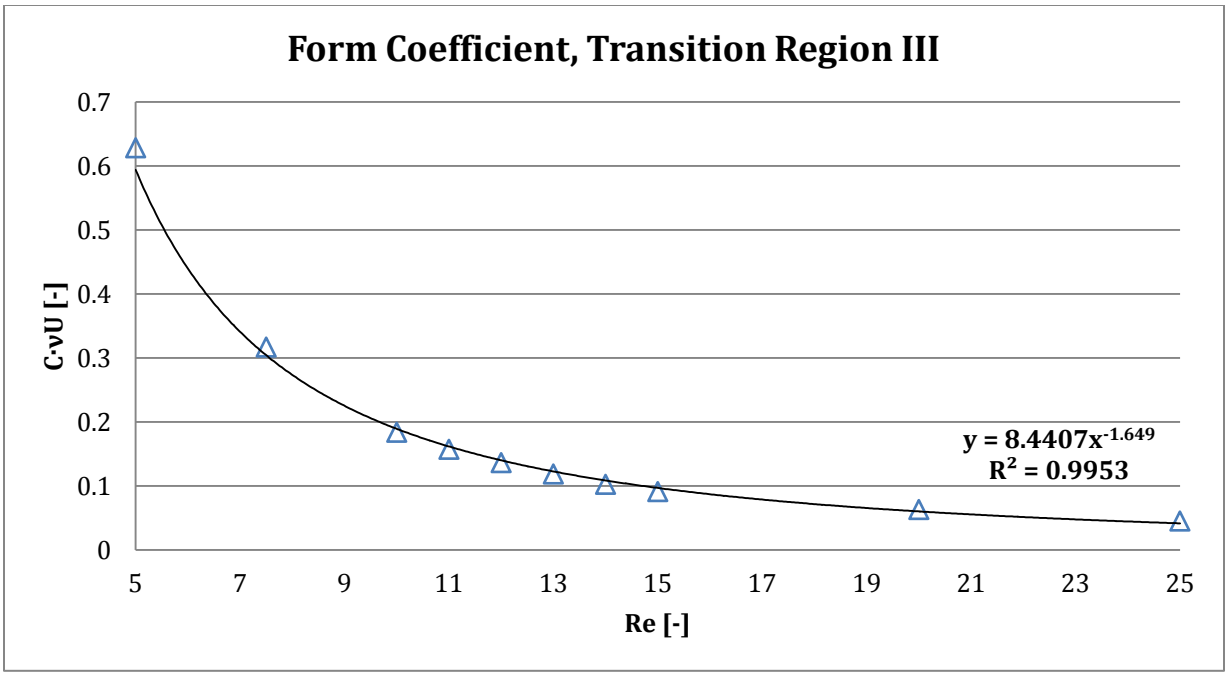


Figure 21. Form coefficient in third region of transition.

The coefficients in the trend line equation are now considerably less than they were in the previous regions of flow, as is the range of plotted values. The form coefficient is now approaching zero, and these data are now less correlated than their previous counterparts like the permeability and reduced pressure drop.

It was mentioned in a previous section that the power law approximation was chosen over a polynomial trend line, but the brief explanation could now use more detail. A polynomial can certainly be used to approximate some trends, but this experiment needed an infinitely smooth approximation for stability purposes. For example, the 5$^{th}$-order polynomial approximation of the form coefficient data from Fig. 21 is shown by Eq. (6.4.1).

$$y = -(2e-6)x^5 + (2e-4)x^4 - .0054x^3 + .0874x^2 - .7316x + 2.675 \qquad (6.4.1)$$

This correlation has a correlation coefficient of almost 1. However, the error involved during its calculation would play a major factor, since decimals are truncated at a certain number of digits (which

depends where and how the software is used). Also, this polynomial will eventually reach negative and positive infinity on the left and right sides, respectively. Infinite values of flow variables are simply not possible, even though Figs. 5, 6, and 7 show asymptotic behavior at extreme values.

Mathematical reasons aside, another reason the polynomial approximation was not used in this experiment was that it is not applicable to the entire data set. There are just simply too many transitions between ranges (hence the separation of regions) for a polynomial to handle. An approximation of the data as a whole would need to be simple as possible and continuous at all values. It is true that exponential functions exhibit this behavior, but the power law provided a much better correlation in all regions and data sets.

Another reason for using the power law approximation is that the laminar boundary layer and jet approximations use the power law, along with the approximation of potential flow. While this study does not explicitly investigate these two phenomena or assume potential flow, they are still under the umbrella of laminar flow approximation with Nek5000.

Potential flow is a method of solving for streamlines—and consequently the velocity profiles—of fluid flow over a body. Several assumptions are made before potential flow can be evaluated. The first of these assumptions is steady laminar flow. Nek5000 is indeed a laminar flow solver, but in order to find a steady flow, a calculation must be allowed to converge in a similar manner to the results of this study. Incompressibility is not an issue for Nek5000, since it is natively supported. However, irrotational flow is realistically impossible to produce, because any disturbance at all causes a flow to have some degree of rotation.

During the derivation of some potential flow solutions, it is appropriate to assume that the velocity profiles have the form of a power function, or power law. The power law profile provides the basic profile of laminar boundary layer, jets, and wakes. For example, the boundary layer thickness, $\delta$, is proportional to the square root of the distance along the no-slip surface. Equation (7.1) shows the relation between $\delta$ and distance along a stationary plate in laminar boundary layer flow. With a constant value for kinematic viscosity and mean flow speed, this equation is essentially a power law.

$$\delta_{.99} = 4.92\sqrt{\nu x/_U} \tag{7.1}$$

Perhaps a more appropriate comparison would be the velocity profile along the surface of a cylinder in potential flow. The experiment performed earlier contains such a cylinder in the center of the mesh. Schlicting [12] stipulates that a high-order (up to 11) power law series is needed to approximate flow past a cylinder. Such a power law series has the form of Equation (7.2), where $u_1 = 2\frac{U_\infty}{R}$, $u_3 = -\frac{2U_\infty}{3!R}$, and so forth.

$$U(x) = u_1 x + u_3 x^3 + u_5 x^5 + \cdots u_n x^n \tag{7.2}$$

As mentioned, Schlicting carries this series out to 11, and uses it with a similarity solution to obtain the plot seen in Figure 22. The variable of the vertical axis can be more simply expressed as $\eta$, a common choice for a similarity variable. Also, each separate profile was evaluated at a distinct angle along the cylinder surface. The method of how these angles were measured is also included in Fig. 22.

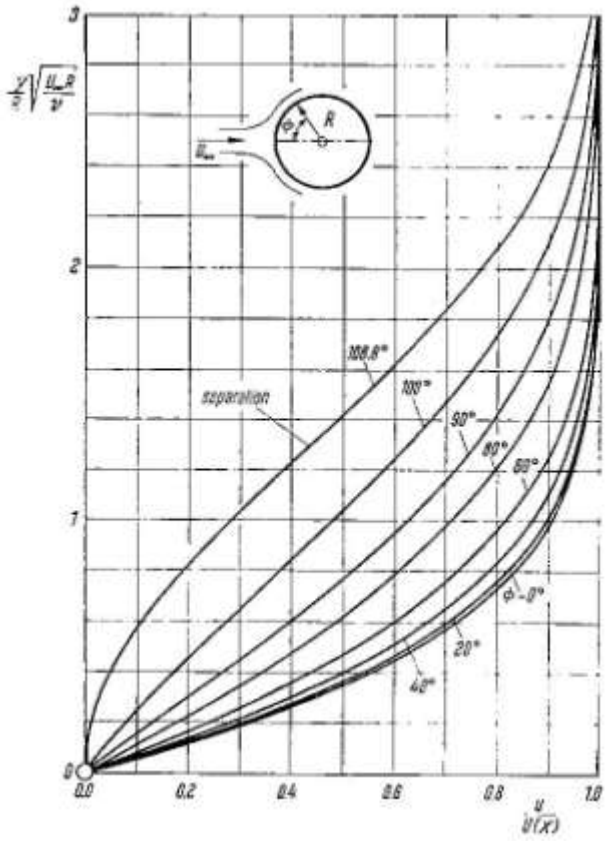


Figure 22. Similar velocity profiles of flow past cylinder.

Here, the angle of separation has been predicted at 108.8 degrees. Many experiments to validate these profiles have been conducted since the inception of this work, and Nek5000 does not show any obvious deviations from the work by Schlicting.

Even though the profiles in Fig. 22 are from a power law, they would not accurately reflect the results of this experiment. Recall that the profiles in Fig. 22 are for potential flow over a single cylinder. The symmetry boundary conditions on the floor and ceiling of the mesh prevent Schlicting's exact solution to occur in a Nek5000 experiment. In order to properly compare the current results to Fig. 22, an accurate boundary layer profile must first be seen. The Lineout mode was used at an angle of 90 degrees to compare the boundary layer velocity profile to the similarity solution in Fig. 22. Figure 23 is plot of this velocity profile for all applied Reynolds numbers, and is measured from the top of the center cylinder to

the ceiling of the test section. Keep in mind that Nek5000 was used in a non-dimensional form for this thesis, so a horizontal velocity value of 1.0 is really the ratio of local velocity to the free stream velocity.

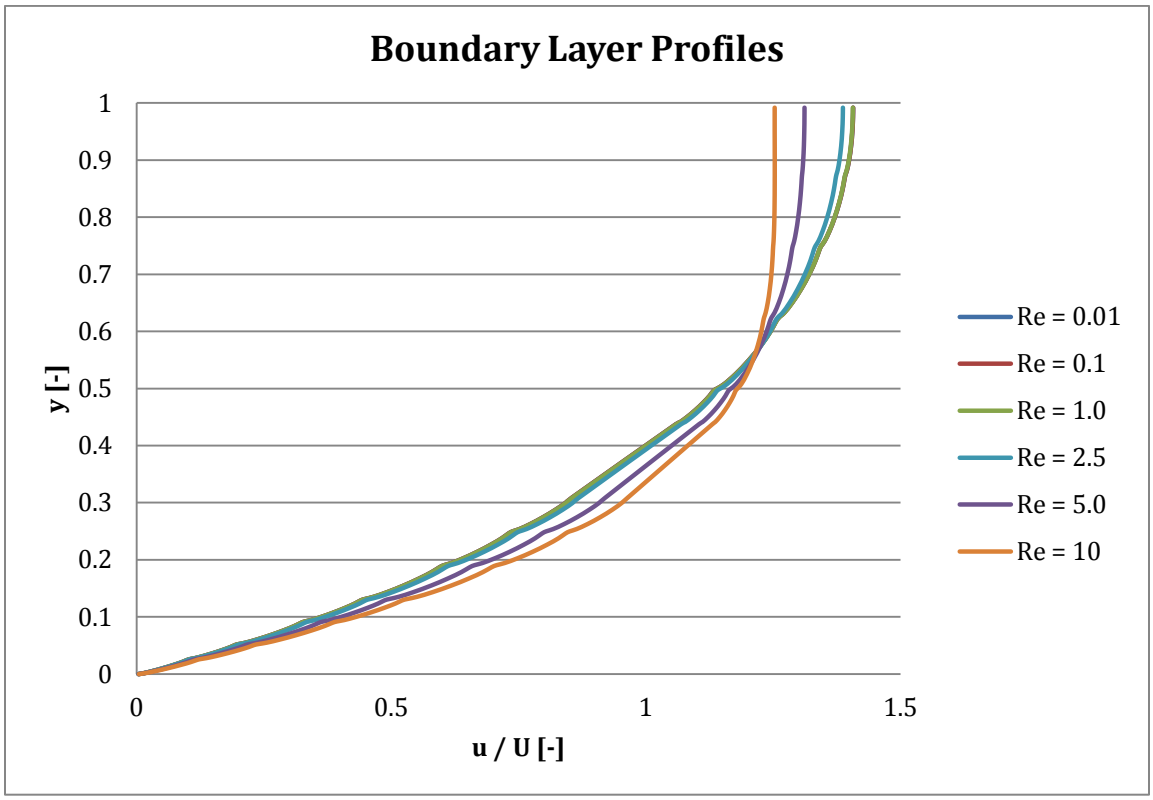


Figure 23. Boundary layer profiles at ϕ = 90°.

These profiles were expected, and one can see that they follow the similarity solution of $\eta$ presented in Fig. 22. One of the distinct features of this profile is the approximately constant slope of the profiles when the velocity ratio is between zero and 0.5. The other is the behavior at the farthest distance from the surface, where the velocity ratio is approaching a constant. This is indicative of flow outside the boundary layer.

The development of the boundary layer along the surface is now under consideration. To begin, the Reynolds number is held constant at 0.01, because this regime falls within the restrictions of the flow across both a single cylinder and porous media. Figure 24 shows how the boundary layer develops from stagnation (ϕ = 0°) to 130°.

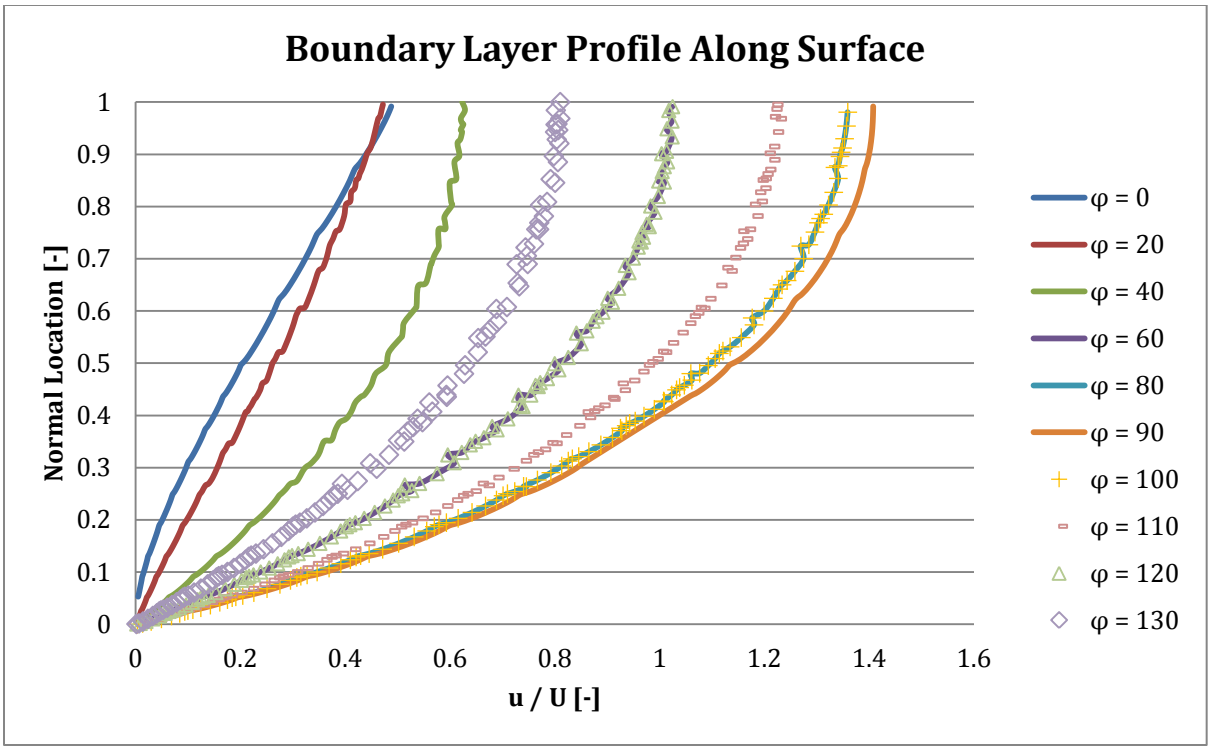


Figure 24. Boundary layer development when *Re* = 0.01.

Figure 24 contains a large amount of data, but the visible trend is that the profiles begin to regress back to stagnation after 90 degrees. Nek5000 is not allowing much separation, if any at all, to occur at such a low Reynolds number. If a single cylinder was being investigated instead of a porous medium unit cell, then one might conclude that the Stokes regime is being entered.

# Chapter 7: Conclusions and Recommendations

One of the themes that resounded throughout this experiment is that the laminar Nek5000 solver exhibited stability through all applied regions of flow. Perturbations were not employed, which would certainly cause instabilities if used.

The reduced pressure drop is now confirmed to have a strong correlation with the applied Reynolds number. The results of the previous chapter showed this strong correlation for each separate region and for the overall data set as well. However, the correlations in the separate regions of flow were stronger. This requires any future implementations of these results to accommodate for the changing trend line equations.

The boundary layer behavior calculated by Nek5000 is close to the ideal similarity solution, but is found in a much different way. The reason that similarity solutions existed was to evaluate potential flow with far less computing resources than what is available today.

Based on the results of this thesis, the future implementation of Nek5000 as a porous media solver looks bright. Nek5000 gives strong correlations between the Reynolds number and the reduced pressure drop, permeability, and form coefficient (in their dominant / desired regions of course). The drag ratio plotted in Fig. 8 needs to be evaluated with a better method, possibly in real dimensions. Nek5000 is capable of dimensional calculations, but the computational cost is significantly higher.

The first recommendation for this study is to investigate the spikes of pressure found at the upper and lower corners of the inlet. Figure 25 shows a close-up view of the upper corner of the inlet at a Reynolds number of 1.6.

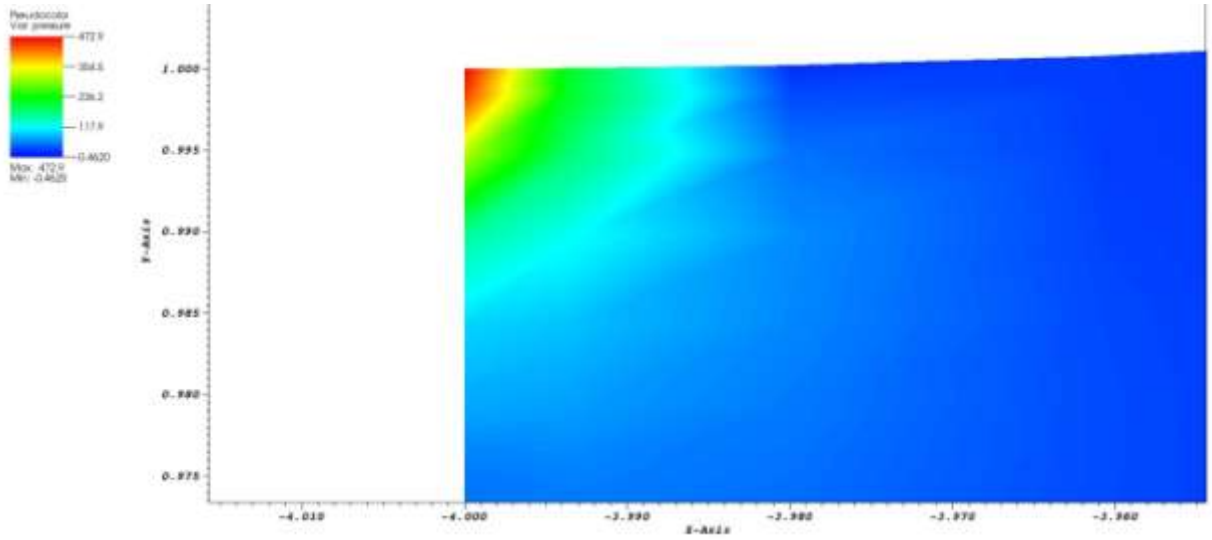

Figure 25. Close-up view of high pressure region found at inlet at *Re* = 1.6.

The effect was determined to be negligible because it quickly fades away from the cylinder wall, but if wall effects are ever evaluated, this phenomenon may need to be addressed. It is possibly an undesired effect of the inlet boundary condition used by Nek5000. For comparison, Figure 26 shows a similar phenomenon at a Reynolds number of 0.01. Note the larger values of pressure indicated by the legend.

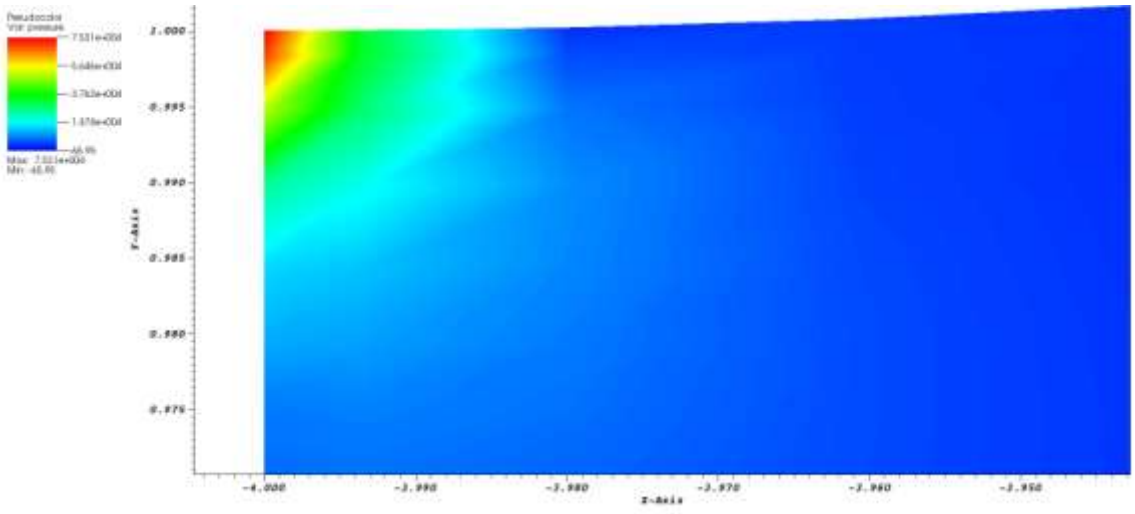

Figure 26. Close-up view of high pressure region found at inlet at *Re* = 0.01.

This effect certainly fades as one moves away from the corner, but it is not clear if affects the calculation of pressure at the center line or not. Further investigation is needed to confirm the cause and possible remedy of this phenomenon.

The meshing utility Prenek is not as user-friendly as others that are presently available. Unfortunately, Prenek was the only option available for this study, and it proved to be extremely time consuming. Nodal placement is done manually, unlike many other mesh generators such as ICEM or Cubit.

The use of Eqs. (4.1.5) and (4.1.8) may yield more accurate results, but they require separate test sections of porous and non-porous media. This is not an unachievable task, even in Prenek, but the time required to create and conform that mesh in Prenek may prove to be even more time-consuming than the mesh used in this study. As mentioned in the previous paragraph, more advanced mesh generators would create a combined mesh with relative ease. However, the boundary conditions used by Nek5000 become troublesome when applied to unstructured meshes.

The final recommendations would be to extend the correlations found in this thesis to a laminar porous media Nek5000 model, and possibly into turbulence models. Since Nek5000 is relatively unique in the way it performs calculations, it would be preferable to use its infrastructure with its own results. This is especially true in the current turbulence model available in Nek5000, which uses Large-Eddy Simulation (LES) to approximate turbulence. The investigation of packed-bed structures with Nek5000 is already under way by other researchers, and a porous media model would be one of the next steps toward a full thermal-hydraulic reactor model.

# References


[1] Nek5000 Primer. Web. 14 October 2014. http://nek5000.mcs.anl.gov

[2] Ortensi, J., Strydom, G., Sen, R. Sonat, Pope, M. A., Bingham, A., Gougar, H., Seker, V., Collins, B., Downar, T., Ellis, C., Baxter, A., Vierow, K., Clifford, I. D., Ivanov, K., DeHart, M. "Prismatic Coupled Neutronics Thermal Fluids Benchmark Definition." *In Publication.* OECD/NEA. Paris (2012).

[3] Chandesris, M., Serre, G., Sagaut, P. "A macroscopic turbulence model for flow in porous media suited for channel, pipe and rod bundle flows." International Journal of Heat and Mass Transfer. 49. 15-16 (2006): 2739-2750.

[4] Pedras, M.H.J., and de Lemos, M.J.S. "On the definition of turbulent kinetic energy for flow in porous media." International Communications of Heat and Mass Transfer. 27. 2 (2000) 211-220.

[5] Clifford, Ivor D. *A Hybrid Coarse and Fine Mesh Solution Method for Prismatic High Temperature Gas-Cooled Reactor Thermal-Fluid Analysis.* Dissertation. The Pennsylvania State University, 2013. Web. 8 June 2015.

[6] Narasimhan, Arunn. *Essentials of Heat and Fluid Flow in Porous Media.* Boca Raton: CRC Press, 2013. Print.

[7] de Lemos, Marcelo J.S. *Turbulence in Porous Media: Modeling and Applications.* Kidlington: Elsevier, 2006. Print.

[8] Pedras, M.H.J., and de Lemos, M.J.S. "On the Mathematical Description and Simulation of Turbulent Flow in a Porous Medium Formed by an Array of Elliptic Rods." Journal of Fluids Engineering. 123. (2001) 941-947.

[9] Nek Users' Guide. Web. 13 January 2016. http://nek5000.mcs.anl.gov

[10] Kundu, Pijush K., Cohen, Ira M., and Dowling, David R. *Fluid Mechanics.* Elsevier: Academic Press, 2012. Print.

[11] Lage, Jose L., Krueger, Paul S., and Narasimhan, Arunn. "Protocol for measuring permeability and form coefficient of porous media." Physics of Fluids. 17. 088101 (2005).

[12] Schlicting, Hermann. *Boundary-Layer Theory.* United States: McGraw-Hill, Inc. 1979. Print.

# Appendix A – Design Parameters of the MHTGR-350 Standard Fuel Element

| Fuel Element Geometry | Value | Units |
|---|---|---|
| Block graphite density (for lattice calculations) | 1.85 | $g/cm^3$ |
| Fuel holes per element | | |
| Standard element | 210 | |
| RSC element | 186 | |
| Fuel hole radius | 0.635 | cm |
| Coolant holes per element (large/small) | | |
| Standard element | 102/6 | |
| RSC element | 88/7 | |
| Large coolant hole radius | 0.794 | cm |
| Small coolant hole radius | 0.635 | cm |
| Fuel/coolant pitch | 1.8796 | cm |
| Block pitch (AF distance) | 36 | cm |
| Element length | 79.3 | cm |
| Fuel handling diameter | 3.5 | cm |
| Fuel handling length | 26.4 | cm |
| RSC hole diameter | 9.525 | cm |
| LBP holes per element | 6 | |
| LBP radius | 0.5715 | cm |
| LBP gap radius | 0.635 | cm |

# Appendix B – Experimental Data

| | | *Pressure* | | | | | |
|---|---|---|---|---|---|---|---|
| NSTEPS | ***Re*** | **Inlet** | **Outlet** | **$\Delta P_r$** | **$K/v^2$** | **C·νU** | **λ** |
| 6.40E+04 | 0.01 | 1216.03 | 22.008 | 1194.02 | 8.38E-06 | 119402.200 | 1.25E-03 |
| 5.00E+04 | 0.02 | 609.01 | 11.060 | 597.95 | 3.34E-05 | 29897.545 | 2.50E-03 |
| 5.00E+04 | 0.03 | 405.61 | 7.350 | 398.26 | 7.53E-05 | 13275.452 | 3.75E-03 |
| 5.00E+04 | 0.04 | 304.31 | 5.518 | 298.79 | 1.34E-04 | 7469.868 | 5.00E-03 |
| 5.00E+04 | 0.05 | 243.53 | 4.419 | 239.11 | 2.09E-04 | 4782.261 | 6.25E-03 |
| 5.00E+04 | 0.06 | 203.01 | 3.686 | 199.32 | 3.01E-04 | 3322.082 | 7.50E-03 |
| 4.80E+04 | 0.07 | 174.07 | 3.163 | 170.91 | 4.10E-04 | 2441.520 | 8.75E-03 |
| 5.00E+04 | 0.08 | 152.36 | 2.770 | 149.59 | 5.35E-04 | 1869.900 | 1.00E-02 |
| 5.00E+04 | 0.09 | 135.48 | 2.465 | 133.01 | 6.77E-04 | 1477.926 | 1.13E-02 |
| 5.00E+04 | 0.10 | 121.97 | 2.220 | 119.75 | 8.35E-04 | 1197.516 | 1.25E-02 |
| 5.00E+04 | 0.20 | 61.20 | 1.121 | 60.07 | 3.33E-03 | 300.371 | 2.50E-02 |
| 5.00E+04 | 0.30 | 40.94 | 0.755 | 40.18 | 7.47E-03 | 133.948 | 3.75E-02 |
| 5.00E+04 | 0.40 | 30.81 | 0.572 | 30.24 | 1.32E-02 | 75.605 | 5.00E-02 |
| 5.00E+04 | 0.50 | 24.74 | 0.462 | 24.28 | 2.06E-02 | 48.556 | 6.25E-02 |
| 5.00E+04 | 0.60 | 20.69 | 0.389 | 20.30 | 2.96E-02 | 33.840 | 7.50E-02 |
| 5.00E+04 | 0.70 | 17.80 | 0.337 | 17.47 | 4.01E-02 | 24.953 | 8.75E-02 |
| 5.00E+04 | 0.80 | 15.64 | 0.297 | 15.34 | 5.21E-02 | 19.177 | 1.00E-01 |
| 5.00E+04 | 0.90 | 13.96 | 0.267 | 13.69 | 6.57E-02 | 15.211 | 1.13E-01 |
| 5.00E+04 | 1.00 | 12.61 | 0.243 | 12.37 | 8.08E-02 | 12.372 | 1.25E-01 |
| 5.00E+04 | 1.10 | 11.50 | 0.223 | 11.28 | 9.75E-02 | 10.256 | 1.38E-01 |
| 5.00E+04 | 1.20 | 10.21 | 0.200 | 10.01 | 1.20E-01 | 8.340 | 1.50E-01 |
| 5.00E+04 | 1.30 | 9.84 | 0.193 | 9.65 | 1.35E-01 | 7.420 | 1.63E-01 |
| 5.00E+04 | 1.40 | 9.18 | 0.182 | 9.00 | 1.56E-01 | 6.430 | 1.75E-01 |
| 5.00E+04 | 1.50 | 8.62 | 0.171 | 8.44 | 1.78E-01 | 5.630 | 1.88E-01 |
| 5.00E+04 | 1.60 | 8.12 | 0.163 | 7.96 | 2.01E-01 | 4.975 | 2.00E-01 |
| 5.00E+04 | 1.70 | 7.69 | 0.155 | 7.53 | 2.26E-01 | 4.431 | 2.13E-01 |
| 5.00E+04 | 1.80 | 7.30 | 0.148 | 7.15 | 2.52E-01 | 3.975 | 2.25E-01 |
| 5.00E+04 | 1.90 | 6.96 | 0.142 | 6.82 | 2.79E-01 | 3.588 | 2.38E-01 |
| 5.00E+04 | 2.50 | 5.49 | 0.116 | 5.38 | 4.65E-01 | 2.152 | 3.13E-01 |
| 5.00E+04 | 5.00 | 3.21 | 0.068 | 3.14 | 1.59E+00 | 0.629 | 6.25E-01 |
| 5.00E+04 | 7.50 | 2.43 | 0.048 | 2.38 | 3.15E+00 | 0.317 | 9.38E-01 |
| 7.50E+04 | 10.00 | 1.88 | 0.041 | 1.84 | 5.43E+00 | 0.184 | 1.25E+00 |
| 7.50E+04 | 11.00 | 1.77 | 0.037 | 1.73 | 6.35E+00 | 0.157 | 1.38E+00 |
| 7.50E+04 | 12.00 | 1.67 | 0.035 | 1.64 | 7.32E+00 | 0.137 | 1.50E+00 |
| 8.00E+04 | 13.00 | 1.58 | 0.033 | 1.55 | 8.41E+00 | 0.119 | 1.63E+00 |

| | | | | | | | |
|---|---|---|---|---|---|---|---|
| 1.00E+05 | 14.00 | 1.47 | 0.032 | 1.44 | 9.73E+00 | 0.103 | 1.75E+00 |
| 2.50E+05 | 15.00 | 1.40 | 0.034 | 1.37 | 1.09E+01 | 0.091 | 1.88E+00 |
| 9.90E+05 | 20.00 | 1.31 | 0.039 | 1.27 | 1.58E+01 | 0.063 | 2.50E+00 |
| 1.13E+06 | 25.00 | 1.17 | 0.035 | 1.14 | 2.20E+01 | 0.045 | 3.13E+00 |